1/33

EVALUATION OF FAULTING AS IT RELATES TO POSTCLOSURE PERFORMANCE OF THE PROPOSED HIGH-LEVEL WASTE REPOSITORY AT YUCCA MOUNTAIN, NEVADA

Prepared for

U.S. Nuclear Regulatory Commission
Contract NRC–02–02–012

Prepared by

John A. Stamatakos
David A. Ferrill
Deborah J. Waiting
Alan P. Morris
Darrell W. Sims
Amitava Ghosh

Center for Nuclear Waste Regulatory Analyses
San Antonio, Texas

April 2003

CONTENTS

CONTENTS (continued)

3/33

FIGURES

4/33

TABLES

ACKNOWLEDGMENTS

This report was prepared to document work performed by the Center for Nuclear Waste Regulatory Analyses (CNWRA) for the U.S. Nuclear Regulatory Commission (NRC) under contract No. NRC–02–02–012. The studies and analyses reported here were performed on behalf of the NRC Office of Nuclear Material Safety and Safeguards, Division of Waste Management. The report is an independent product of the CNWRA and does not necessarily reflect the views or regulatory position of the NRC.

The authors wish to thank B. Hill for a thorough technical review and useful insights, B. Long for editorial expertise, B. Sagar for programmatic review, and B. Caudle for format review. The administrative and format support provided by R. Emmot is also appreciated. Cross-checking of references provided by K. Murphy is acknowledged.

QUALITY OF DATA, ANALYSES, AND CODE DEVELOPMENT

DATA: CNWRA data contained in this report meet quality assurance requirements described in the CNWRA Quality Assurance Manual. Data used to support conclusions in this report taken from documents published by the U.S. Department of Energy (DOE) contractors and supporting organizations were generated according to the quality assurance program developed by DOE for the Yucca Mountain Project.

ANALYSES AND CODES: Maps and related Geographic Information System (GIS) data were generated and plotted by the software ArcView GIS© Versions 3.1 (ESRI, 1998) and 3.2a (ESRI, 2000), which are commercially available software codes that are maintained in accordance with CNWRA Technical Operating Procedure TOP–018. Total system performance analyses were conducted using the Total-system Performance Assessment (TPA) Version 4.1j code[1] (Mohanty, et al., 2002), including the EBSREL, EBSFAIL, and NFENV modules, which are included in the TPA Version 4.1j code as well as the FAULTO module (Ghosh, et al., 1997). The TPA Version 4.1j code and FAULTO module were developed at the Center for Nuclear Waste Regulatory Analyses in accordance with CNWRA Technical Operating Procedure TOP–018.

References

ESRI. "ArcView GIS©." Version 3.2a. Redlands, California: ESRI. 2000.

ESRI. "ArcView GIS©." Version 3.1. Redlands, California: ESRI. 1998.

Ghosh, A., R.D. Manteufel, and G.L. Stirewalt. "Faulting Version 1.0—A Code for Simulation of Direct Fault Disruption: Technical Description and User's Guide. San Antonio, Texas: CNWRA. 1997.

Mohanty, S., T.J. McCartin, and D.W. Esh. "Total-system Performance Assessment (TPA) Version 4.0 Code: Module Description and User's Guide." San Antonio, Texas: CNWRA. 2002.

---

[1] TPA Version 4.0 code is the last iteration of the user's guide. Version 4.1j, however, was used for calculations in this report. Despite several changes to the code in moving from Version 4.0 to 4.1j, the documentation in the user's guide for Version 4.0 remains applicable. Most revisions pertain to replacing old with new data as these were made available through the course of developing this report.

EXECUTIVE SUMMARY

The potential effect of direct fault displacement of the engineered barrier subsystems is one of several disruptive scenarios currently being evaluated by the U.S. Department of Energy (DOE) for postclosure repository performance at Yucca Mountain, Nevada. To address this potential disruptive scenario, DOE is assessing both the probability and consequences of faulting. Probability estimates of future faulting events at Yucca Mountain were developed as part of the DOE expert elicitation on seismicity and faulting. In that elicitation, 18 experts working on six 3-person teams derived probabilistic fault-displacement hazard curves for a series of demonstration points at or near Yucca Mountain. These demonstration points were selected to represent faulting and related fault deformation in the subsurface and near the proposed surface facility sites. DOE is currently using the results of that expert elicitation to evaluate the potential consequences of faulting on repository performance. At present, DOE considers faulting within the repository to be too infrequent and fault displacements too small to impact repository performance and, as such, has screened faulting disruptive events from consideration in its total system performance assessment.

To evaluate the DOE analyses of faulting within a potential License Application for Yucca Mountain, staff reviewed the DOE probabilistic fault displacement results and associated DOE analyses of the potential consequences of faulting. Based on this review of the DOE analyses, and coupled with risk insights gained from consequence analyses of faulting, staff conclude that DOE has assembled sufficient information in the prelicensing period on the issue of direct faulting for U.S. Nuclear Regulatory Commission (NRC) to conduct a review of a potential License Application. Therefore, staff consider the faulting subissue, as defined within the Structural Deformation and Seismicity Key Technical Issue, to be closed.

Staff developed two review methodologies that can be used to evaluate the potential consequences of fault displacement of the waste packages and drip shields. Both methodologies are able to evaluate potential faulting consequences in either an open or backfilled (engineered or due to natural rockfall) repository. The first methodology is based on an abstraction of faulting within the staff TPA Version 4.1j code, using faulting parameters derived from geological data. The second methodology is a more detailed process model based on patterns of primary and secondary faults obtained from historic large-magnitude earthquakes in the Basin and Range. Both methodologies consider only the specific disruptive event of direct fault displacement of the waste packages and drip shields. Other potential effects of faulting, such as fault-induced modifications to groundwater flow, rockfall, or enhanced corrosion of the engineered barrier subsystem because of rock–waste package interaction, are considered separately in other disruptive event analyses.

Review Methodology I abstracts faulting directly into the TPA Version 4.1j code using the FAULTO module. This abstraction simulates a single fault displacement on an existing fault within the repository, such as the Ghost Dance and Solitario Canyon faults, and then calculates the number of waste packages potentially damaged by the fault displacement as those that lie wholly or partially within the fault zone. Fault-zone widths (thickness of fault perpendicular to the fault plane) are sampled from probability distribution functions developed from geological observations of fault zones at Yucca Mountain. The numbers of waste package failures and their locations in the repository are then passed on to other routines in the TPA Version 4.1j code, which calculate the dose release. The analyses are conditional so that a faulting event is forced to occur in each realization of the TPA Version 4.1j code. Risk is then calculated by

weighting the conditional dose by the probability that a faulting event with a given amount of fault displacement will cause waste package failure. Probabilities of fault displacements are taken from the DOE probabilistic fault displacement hazard results.

Review Methodology II evaluates distributed faulting by considering the patterns of surface faulting displacements from historical earthquakes in the Basin and Range physiographic province. In this methodology, a range of fault trace-length densities is computed from four historical earthquakes. The fault trace-length densities were measured as line length of fault trace-length per square kilometer of area. These values of fault trace-length density can be combined with geometrical information about the repository layout, such as drift spacing and drift orientation, to estimate the number of waste packages intersected by the distributed faults. The number of damaged waste packages is then passed on to the TPA Version 4.1j code as juvenile failures, and the code then calculates a conditional dose. These conditional doses are then weighed by the probability that a faulting event with similar fault displacements to the historical analogs would occur at Yucca Mountain. Similar to Methodology I, these probabilities of fault displacements are derived from the DOE probabilistic fault displacement hazard results.

At present, both methodologies rely on various pessimistic or conservative assumptions about the characteristics of faulting and the mechanical behavior of waste packages under faulting loads. These simplifying assumptions are made to develop efficient and understandable abstractions of the natural system. Therefore, results from both methodologies are considered reasonably conservative estimates of the number of potential waste package failures associated with fault displacement.

Insights gained from the application of both methodologies indicate that direct fault disruption of the repository does not appear to contribute significantly to total system risk. Example performance analyses of faulting on the Ghost Dance and Solitario Canyon faults using Methodology I indicate that the risk imposed by faulting on postclosure repository performance is small, on the order of pico-rem to tens of micro-rem per year. Calculated risks are low for this methodology because of the relatively small annual exceedence probabilities for consequential fault displacements at Yucca Mountain (10^{-4} to 10^{-8}/yr) and the relatively few waste packages incorporated in the fault zones. Risk estimates from faulting calculated with Methodology II are similarly small. Using recent earthquakes in the western United States as examples for the style and type of faulting that could occur at Yucca Mountain, performance assessment results suggest pico-rem to micro-rem risks per year.

Therefore, the relatively small risks of faulting support the DOE conclusion that direct faulting of the drifts and waste packages is a disruptive event process that can be screened from total system performance assessment based on low probability and limited consequences. Current analyses suggest solubility limits of the waste material or the probability of faulting would have to increase by several orders of magnitude in order for the risks of faulting to become significant. If faulting is ultimately deemed to make a significant contribution to overall repository risk, the faulting performance assessment methodologies developed in this report will be refined to capture greater realism. If, however, these reasonable upper bound evaluations do not yield significant risks to repository performance, additional realism in the models is not warranted, and staff resources can focus on other more risk-significant issues.

1 INTRODUCTION

1.1 Purpose

This report documents performance assessment methodologies and associated risk information that can be used by staff to evaluate the risk significance of faulting at Yucca Mountain. In particular, the methodologies and risk information described in this report were developed to evaluate potential radiological risks of direct faulting on the postclosure performance of the engineered barrier subsystems at the proposed high-level waste repository at Yucca Mountain. Thus, the analyses and methodologies presented here are directed toward both qualitative and quantitative evaluations of the probability and consequences of faulting on postclosure repository performance.

This report supports two U.S. Nuclear Regulatory Commission (NRC) program objectives. First, results of the faulting analyses coupled with development of the analytical methodologies described herein provide the staff with the necessary technical bases to support issue closure with the U.S. Department of Energy (DOE) during the prelicensing period. The goal of issue closure during this prelicensing period is to assure that DOE has assembled sufficient information for the NRC staff to accept a License Application for review. Closure of technical issues or subissues by the NRC staff during prelicensing does not prevent anyone from identifying technical issues for NRC consideration during the licensing proceedings. In addition, resolution by the NRC staff during prelicensing does not prejudge what the NRC staff evaluation of the issue will be during formal evaluation of a DOE License Application, if and when DOE submits a License Application to the NRC for the proposed Yucca Mountain repository. By definition, subissues of the NRC Key Technical Issues are considered as closed by the NRC staff during prelicensing when the staff have no further questions or comments about how DOE is addressing a technical issue (NRC, 2002a).

Second, the faulting methodologies and results documented in this report will form the technical basis for staff review and assessment of the faulting in a DOE License Application for the proposed Yucca Mountain repository, if and when DOE submits such an application to the NRC. Within the second objective, the analytical methodologies described in this report are consistent with the review methods in NRC (2002b). Analyses presented in this report provide two alternative methodologies to evaluate the risk-significance of faulting to overall repository performance during the postclosure period. Both review methodologies will allow the staff to evaluate the DOE estimates of any potential radiological risks from faulting or any DOE screening arguments used to remove this disruptive event from total system performance assessment calculations.

1.2 Scope

This report is limited to an evaluation of the possible intersections of tectonically active faults with waste packages and drip shields and the potential consequences on repository performance throughout a 10,000-year performance period. This scope is a subset of the more broadly defined disruptive scenarios of faulting as established in the DOE documentation of features, events, and processes (CRWMS M&O, 2000a). The narrow scope of potential faulting effects used in this report excludes other possible coupled effects of faulting, such as fault-induced modifications to groundwater flow, rockfall, or enhanced corrosion of the engineered barrier subsystem due to rock-waste package interaction. These other fault-related

scenarios will be considered and addressed separately in other disruptive event analyses and evaluations.

This report also is limited to analyses of postclosure performance. Review of faulting hazards with respect to preclosure safety and operations will be addressed separately by DOE in preclosure documents planned to be submitted to the NRC prior to licensing, including Topical Report #3.

Abstractions of faulting in the methodologies developed for this report necessarily rely on numerous simplifying assumptions. These assumptions are based on conservative or pessimistic predictions of faulting at Yucca Mountain and the mechanical behavior of waste packages during and after a possible faulting event. The intent in relying on these assumptions was not to establish a worst-case scenario, but to develop the likely risk significance of faulting. This strategy allows evaluation of the possible risks from faulting without devoting relatively large amounts of resources to overly complex performance assessment models. Should these simplified pessimistic models show faulting makes a significant contribution to overall repository risk, the faulting performance assessment methodologies developed in this report will be refined to capture greater realism. If, however, these reasonably conservative evaluations do not show significant risk from faulting to repository performance, additional realism in these models may not be warranted, and staff resources can focus on other more risk-significant issues.

Preliminary performance assessment methodologies and consequence analyses from the FAULTO module previously were documented in Ghosh, et al. (1997) and Mohanty, et al. (2002a). The methodologies and analyses completed for this report build on the evaluations and analyses documented in these earlier reports. Therefore, the methodologies and results presented in this report should be considered to supersede earlier results.

1.3 Background

1.3.1 Geologic Conditions

Yucca Mountain, Nevada, is located within the Walker Lane Belt (Stewart, et al., 1978; Stewart, 1988) near the western edge of the Basin and Range physiographic province. The Yucca Mountain region is characterized by complex interactions of strike-slip and extensional deformation, active for at least the past 65 million years. The physiography resulting from tectonic deformation consists of subparallel north-trending mountain ranges alternating between elongate and internally drained valleys formed through block faulting (Burchfiel, 1965; Stewart, 1988). The ranges are cut by discontinuous northwest-trending right-lateral and east-northeast left-lateral strike-slip faults. The Yucca Mountain region remains tectonically active today, as indicated by Quaternary (i.e., within the last 1.6 Ma) fault displacement (e.g., Simonds, et al.,1995); historic seismicity, including the 1992 Little Skull Mountain earthquake (e.g., Harmsen, 1994); and strain, as recorded by geodetic observation (e.g., Savage, et al., 1994).

Yucca Mountain consists of a series of elongate ridges of late Miocene volcanic strata, bounded by north-trending normal faults and crossed by northwest-trending oblique-slip to dextral strike-slip faults (Day, et al., 1998a,b). The north-trending normal faults dip predominantly to the west and separate crustal blocks of gently to moderately east-dipping late Miocene tuffs. The northwest-trending oblique-slip faults accommodate differential extension on the north-trending

normal faults. These two sets of faults are interpreted to be contemporaneous, based on mutual terminations and secondary structures between them, such as pull-apart basins (Day, et al., 1998a,b). Some northwest-trending faults are also normal faults that accommodate extension in relay ramps between overlapping and corrugated normal fault segments (Ferrill, et al., 1999).

The larger of the north-trending ridge-bounding faults at Yucca Mountain are the Solitario Canyon and Paintbrush Canyon–Stagecoach Road faults. These faults are considered principal faults, which are faults deemed capable of independently generating large-magnitude ($\mathbf{M_W} \geq 5$) earthquakes (dePolo, et al., 1991). Most remaining faults in the Yucca Mountain region are regarded as intra-block secondary faults, which are incapable of independent fault displacement but can slip in order to accommodate crustal deformation initiated by displacements on principal faults (CRWMS M&O, 1998a; U.S. Geological Survey, 1996).

During an earthquake, the largest fault displacements at or near the surface occur on the principal fault. Nevertheless, substantial fault displacements can be distributed on an array of secondary faults in the region surrounding the principal fault (Figures 1-1 and 1-2). These secondary fault displacements reflect complex geometrical and kinematic accommodations of the crustal strains imposed on the rocks during an earthquake. Because both principal and secondary faulting could adversely affect repository performance, both fault types must be considered in the analysis of faulting as a potentially disruptive event.

For strike-slip faults, distributed faulting is commonly developed on both sides of the principal fault trace (Figure 1-1). Secondary faulting in strike-slip fault systems is especially prevalent in restraining or releasing bends, which form when the trajectory of the principal fault bends along its strike. In the example shown in Figure 1-1a, a nest of secondary faults forms an extensional duplex in a releasing bend of the Dasht-e Bayaz fault of Iran (Tchalenko and Ambraseys, 1970). Faulting offshore of central California also includes many secondary faults formed in response to strike slip or oblique slip on the Hosgri fault (McLaren and Savage, 2001) (Figure 1-1b). In three dimensions, faulting on strike-slip faults often is manifest as a complex pattern of strike-slip and dip-slip faults. The block diagram in Figure 1-1c illustrates a flower structure in which the principal fault bifurcates upward to form a pull-apart basin (after Woodcock and Fischer, 1986). The cross section in Figure 1-1d shows the resulting complex fault geometry of a strike-slip pull-apart basin, which developed in an analog sandbox model of strike-slip deformation (Sims, et al., 1999).

For dip-slip faults, especially normal faults, secondary faulting is often better developed in the hanging wall of the principal fault (Figure 1-2a through 1-2e). Dip-slip faults at Yucca Mountain exhibit a variety of deformational styles that are represented by the illustrations in Figure 1-2b through 1-2e. In the case of the Borah Peak earthquake, strain in the hanging wall of the Lost River fault (Crone, et al., 1987) includes both extension and contraction in a manner similar to that depicted in Figure 1-2d.

1.3.2 Faulting Hazard Assessments

A deterministic approach is the simplest way to evaluate faulting hazard. This approach was used predominantly before 1998 in the siting of nuclear reactors and other critical facilities. In this approach, faults deemed capable of active deformation are avoided by adequate setback distances. The proposed repository at Yucca Mountain (CRWMS M&O, 2002) is, however,

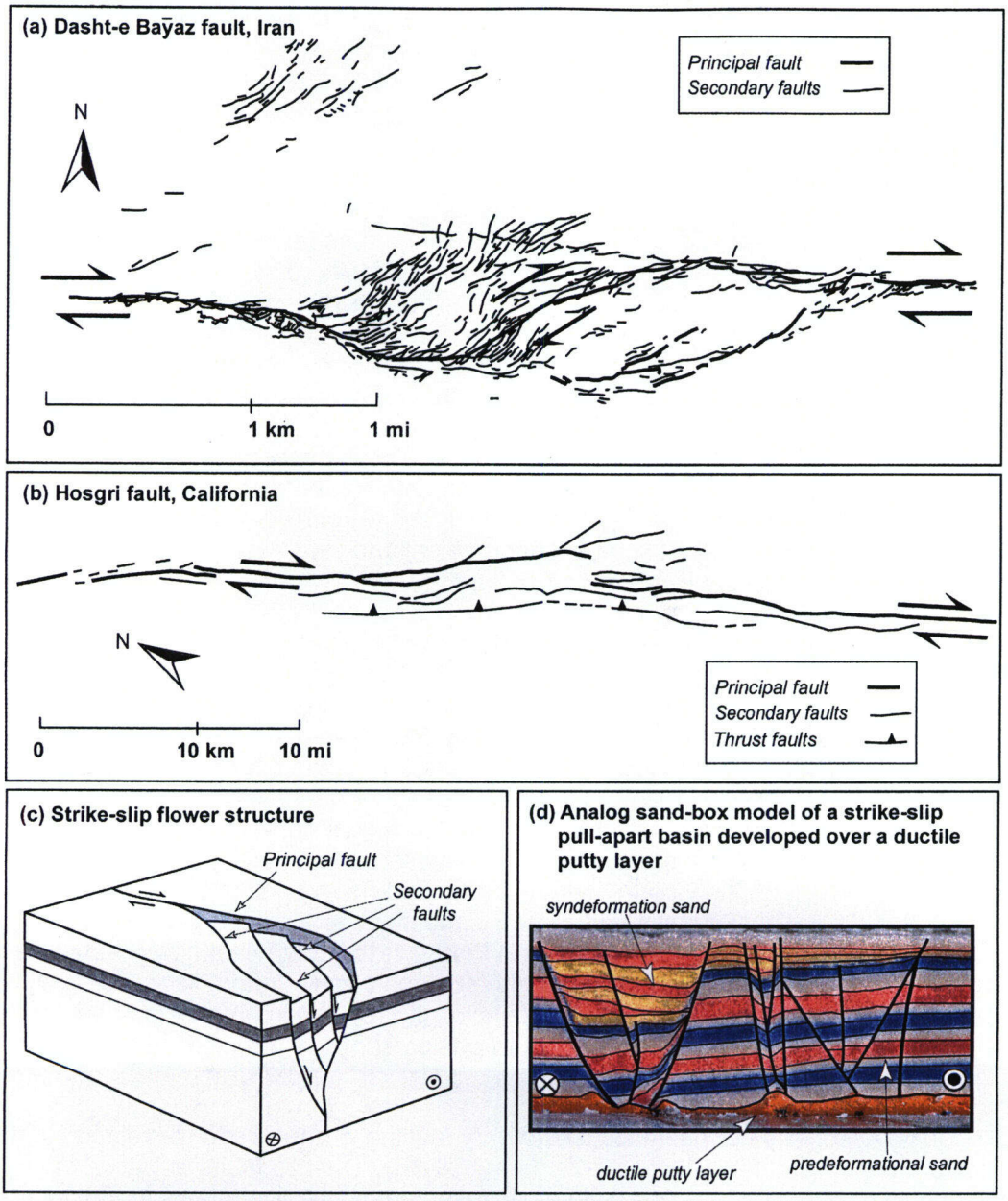

Figure 1-1. Principal and Secondary Faults in Strike-Slip Settings. The Map Pattern of Faults in (a) Is Based on the Detailed Map of Fault Scarps and Fractures Produced Along the Dasht-e Bayaz Fault in Iran (Tchalenko and Ambraseys, 1970). The Map in (b) Is a Fault Map of the Hosgi Fault in California, Modified from Mclaren and Savage (2001). The Block Diagram in (c) Is Derived from Woodcock and Fischer (1986), and It Illustrates a Flower Structure of Secondary Faults That are Common Along Strike-Slip Faults. The Cross Section in (d) Is an Interpretation of Faults in a Pull-Apart Basin Developed in Analog Experiments Using Sand (Sims, et al., 1999). The Interpreted Faults are Overlain on a Photograph of a Vertical Slice of the Analog Model that Was Cut Across the Analog Pull-Apart Basin.

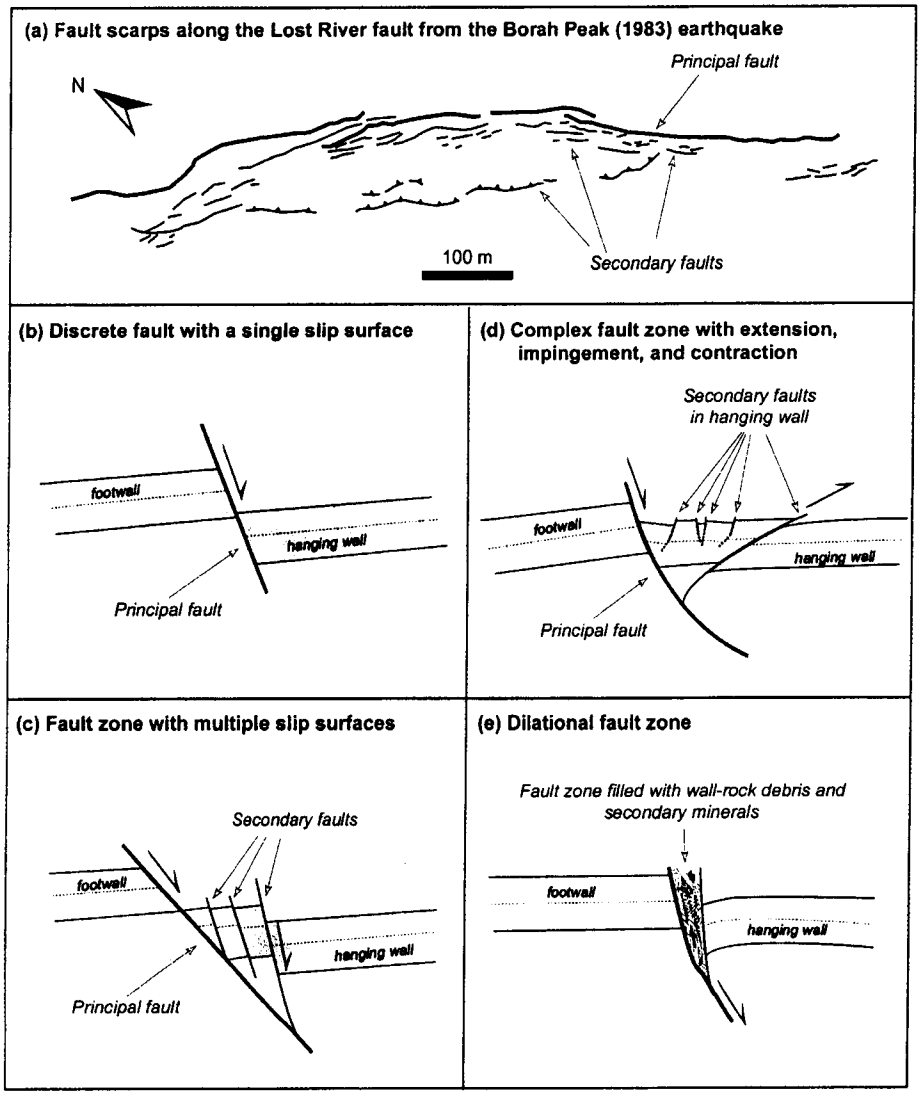

Figure 1-2. Formation of Principal and Secondary Faults Commonly Found in Extensional Tectonic Settings. The Map Pattern of Faults in (a) Is Based on the Detailed Map of Fault Scarps Produced Along the Lost River Fault by the 1983 Borah Peak Earthquake, after Crone, et al. (1987). The Schematic Cross Sections in (b) Through (e) Illustrate Principal and Secondary Faulting. These Types of Principal and Secondary Faults are Commonly Observed at Yucca Mountain, Nevada.

spatially too extensive (Figure 1-3) to reasonably expect that all faults of potential concern can be completely avoided though setback distances (Coppersmith, 1996). Thus, a deterministic approach cannot adequately evaluate potential faulting hazards at Yucca Mountain.

To assess the potential faulting hazard at Yucca Mountain, DOE developed a probabilistic fault displacement hazard assessment as part of the larger probabilistic seismic hazard expert elicitation (CRWMS M&O, 1998a). A recent summary of the DOE probabilistic fault displacement hazard assessment can be found in Youngs, et al. (2003). In the DOE probabilistic fault displacement hazard assessment, individual fault displacement hazard curves, analogous to seismic hazard curves, were developed for principal and secondary faults at Yucca Mountain (Figure1-4). These fault displacement hazard curves plot the fault displacements as a function of estimated annual exceedence probabilities.

For principal faults, the probabilistic fault displacement hazard curves were largely based on the same detailed paleoseismic and earthquake data used in the probabilistic seismic hazard assessment (Youngs, et al., 2003; CRWMS M&O, 1998a; Youngs and Coppersmith, 1985). For secondary faults, however, no established techniques or data were available to the experts that adequately characterize the probability of distributed faulting. Because of the complexity of fault analyses at Yucca Mountain, the experts relied on both anecdotal evidence and expert judgment to develop conceptual models of distributed faulting and to estimate the probabilities of secondary faulting in the repository (Youngs, et al., 2003; CRWMS M&O, 1998a).

One critical aspect in these types of probabilistic analyses is the technical basis for estimates of fault activity or recurrence. Recurrence relationships of faulting are generally derived from paleoseismic data of faults exposed in alluvial trenches. Trenching studies find datable stratigraphic markers offset by faulting events. From the age and amount of fault offset, the recurrence rates for fault displacements can be determined. Recurrence data for faults are then used in conjunction with regional seismicity parameters, such as frequency of earthquakes, to develop probabilistic fault displacement hazard curves for each fault of interest. The curves are derived from two different models: faulting-occurrence and magnitude-occurrence. These methodologies, as applied in the DOE probabilistic seismic hazard assessment (CRWMS M&O, 1998a), have been referred to respectively as the *displacement approach* and the *earthquake approach*. The first approach uses fault-specific data, such as cumulative displacement, fault length, paleoseismic data from trenches, and historic seismicity. The second approach relates the frequency of fault-slip events to the frequency of earthquakes in seismic sources defined in the seismic source models developed for the corresponding seismic hazard analysis.

1.3.3 Faulting Consequence Analyses

Methodologies to assess the potential consequence of direct faulting at Yucca Mountain are not as developed as the faulting hazard assessment. In the total system performance assessments conducted by DOE to date, including performance assessments for the Viability Assessment (CRWMS M&O, 1998b) and the Site Recommendation (CRWMS M&O, 2000a), direct faulting of the subsurface engineered systems was screened out of the assessments based on low probability and design criteria. DOE concluded that the probability of new faulting in the repository was less than the 10^{-8}/yr postclosure regulatory cuttoff. DOE also indicated that appropriate setback would be included in the repository design to mitigate the effects of fault displacement on known faults, especially for the Solitario Canyon fault. DOE, however, continues to assess any potential consequences of faulting at Yucca Mountain to account for

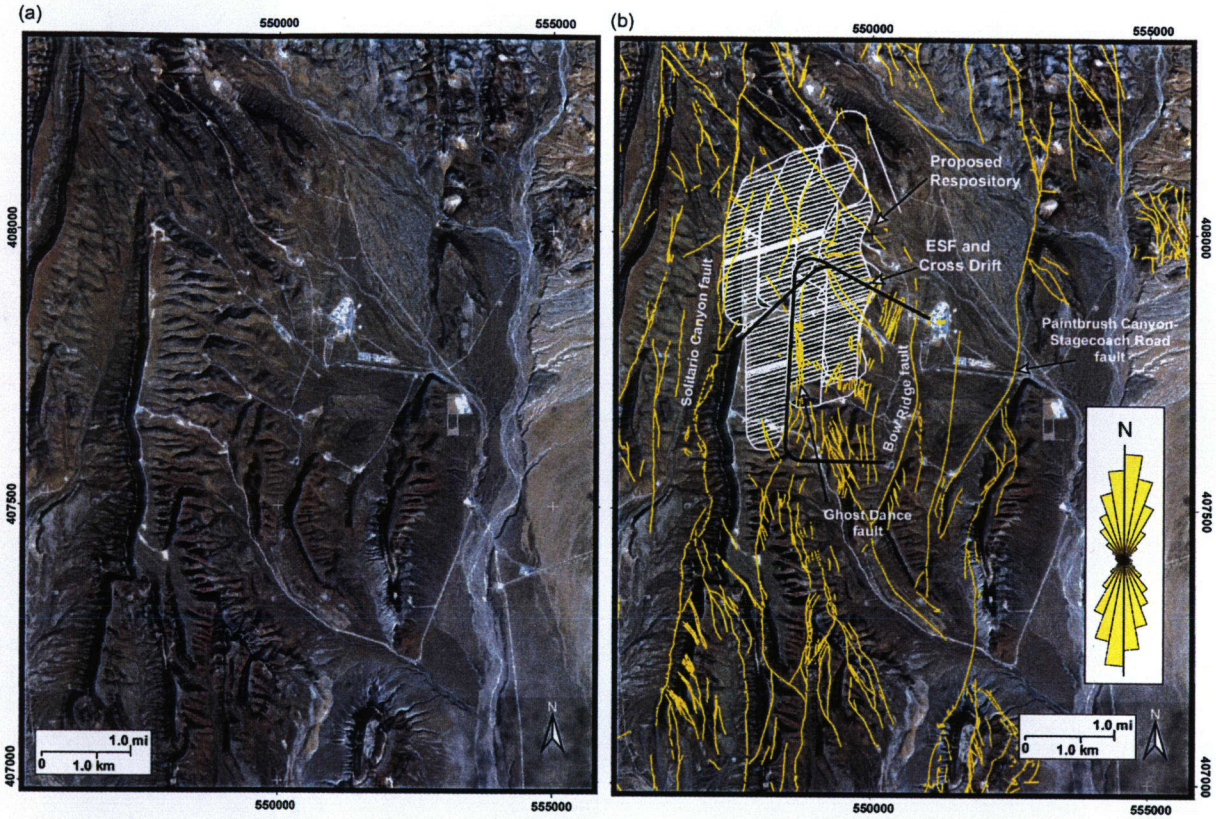

Figure 1-3. Natural Color Mosaic of IKONOS2 Satellite Images Showing the Yucca Mountain Area. The Images Were Captured Between September 2000 and August 2002 and Consist of Panchromatic Sharpened Multispectral Data. Figure (a) Shows Yucca Mountain and the Surrounding Area. Figure (b) Overlays Faults (Yellow Lines) from Simonds, et al. (1995), the Exploratory Studies Facility (ESF), Cross Drift, and Proposed Repository Layout from CRWMS M&O (2002). The Inset Rose Diagram Shows Cumulative Fault Length in Bins of 10-Degree Strike Azimuths. Coordinates Are in Universal Transverse Mercator (UTM) Zone 11, Using the North American Datum of 1927.

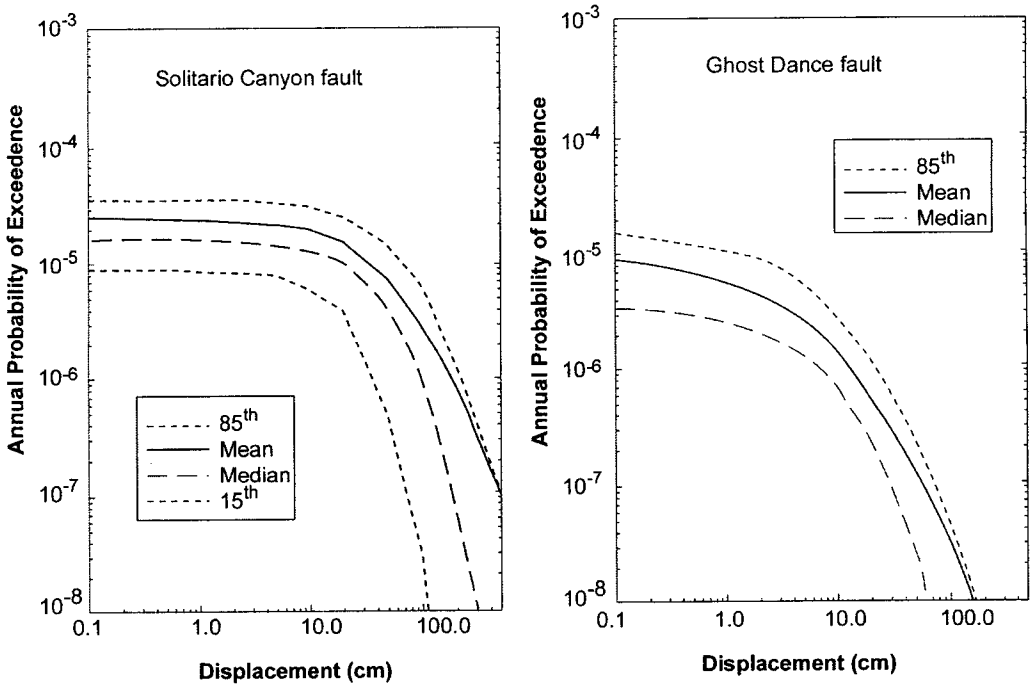

Figure 1-4. Probabilistic Fault Displacement Hazard Assessment Curves for the Solitario Canyon and Ghost Dance Faults. Images were Scanned from CRWMS M&O (1998a) and Reformatted. To Convert to English Units, Multiply Displacements by 0.39 in/cm.

new observations, uncertainties in repository design, and prelicensing agreements with the staff.

In the NRC/CNWRA TPA Version 4.1j code, faulting is evaluated using the FAULTO module, which was derived from the stand-alone faulting program. Preliminary performance assessment methodologies and results from the FAULTO module have been reported in Ghosh, et al. (1998) and Mohanty, et al. (2002b). In both of those preliminary evaluations, the direct consequences of faulting (e.g., intersection of waste packages) did not appear to be significant to postclosure repository performance, especially when compared with other disruptive events of volcanism and seismically induced rockfall. This report provides an updated and more comprehensive evaluation of the consequences of faulting than those earlier reports. In particular, the methodologies and results presented in this report include more recent results from the DOE mapping of faults in the Exploratory Studies Facility and Cross Drift, and the methodologies and results presented in this report directly incorporate the DOE probabilistic fault displacement hazard assessment results. In addition, these new methodologies are based on more realistic conceptual models of faulting.

2 EVALUATION OF THE DOE APPROACH TO FAULTING

2.1 The DOE Probabilistic Fault Displacement Hazard Assessment

Fault displacement hazard analyses assess the probability of slip along faults at Yucca Mountain. Fault slip was evaluated for primary faults and for secondary faults and fractures in which slip could be potentially triggered by an earthquake on a primary fault. DOE developed a probabilistic fault displacement hazard analysis for the repository and surrounding regions of Yucca Mountain (CRWMS M&O, 1998a). The probabilistic fault displacement hazard assessment was constructed as part of the probabilistic seismic hazard analysis expert elicitation. The probabilistic fault displacement hazard assessment used both the displacement and earthquake approaches to develop individual faulting hazard curves (Youngs, et al., 2003). In the expert elicitation (CRWMS M&O, 1998a), probabilistic fault displacement hazard curves were developed for nine representative sites (referred to as demonstration points) at Yucca Mountain (Figure 2-1a and Table 2-1). Of these, points 1, 2, and 3 are on primary faults, points 4, 5, and 6 are on secondary inter-block faults, points 7 and 8 are on small fault zones within the repository footprint, and point 9 is in Midway Valley near the site of the proposed surface facility site.

For both earthquake and displacement approaches, two critical parameters were developed by the expert teams. One parameter describes the amount of likely fault displacement for each faulting event. The second parameter describes how frequent faulting events are likely to occur (Youngs, et al., 2003). Unlike the seismic hazard assessment, methods to develop these faulting parameters are not well established as standard practice; the probabilistic fault displacement hazard assessment methodology essentially was developed by the experts within the DOE probabilistic seismic hazards assessment (CRWMS M&O, 1998a). Thus, the expert teams relied on a wide variety of data and models to develop these two parameters.

Of these two faulting hazard methodologies, the displacement approach is more straightforward because it relies on geologic evidence of prior faulting. The two required parameters can be derived directly from paleoseismic displacement and recurrence-rate data, geologically derived slip-rate data, or scaling relationships that relate displacement to fault length and cumulative fault displacement (e.g., Wells and Coppersmith, 1994).

The earthquake approach uses earthquake recurrence models from the seismic hazard analysis. Three probabilities were assessed in CRWMS M&O (1998a): the probability that (i) an earthquake will occur on a modeled fault, (ii) this earthquake will produce surface displacement on the fault generating the earthquake (the primary fault where the earthquake occurs), and (iii) the earthquake will produce distributed surface displacement on other faults, primary or secondary.

(i) The probability that an earthquake will occur was derived from the DOE seismic hazard assessment. In that assessment, the frequency distribution of an earthquakes for each source (fault or area) was derived from available geologic, historical seismic, or paleoseismic data (CRWMS M&O, 1998a).

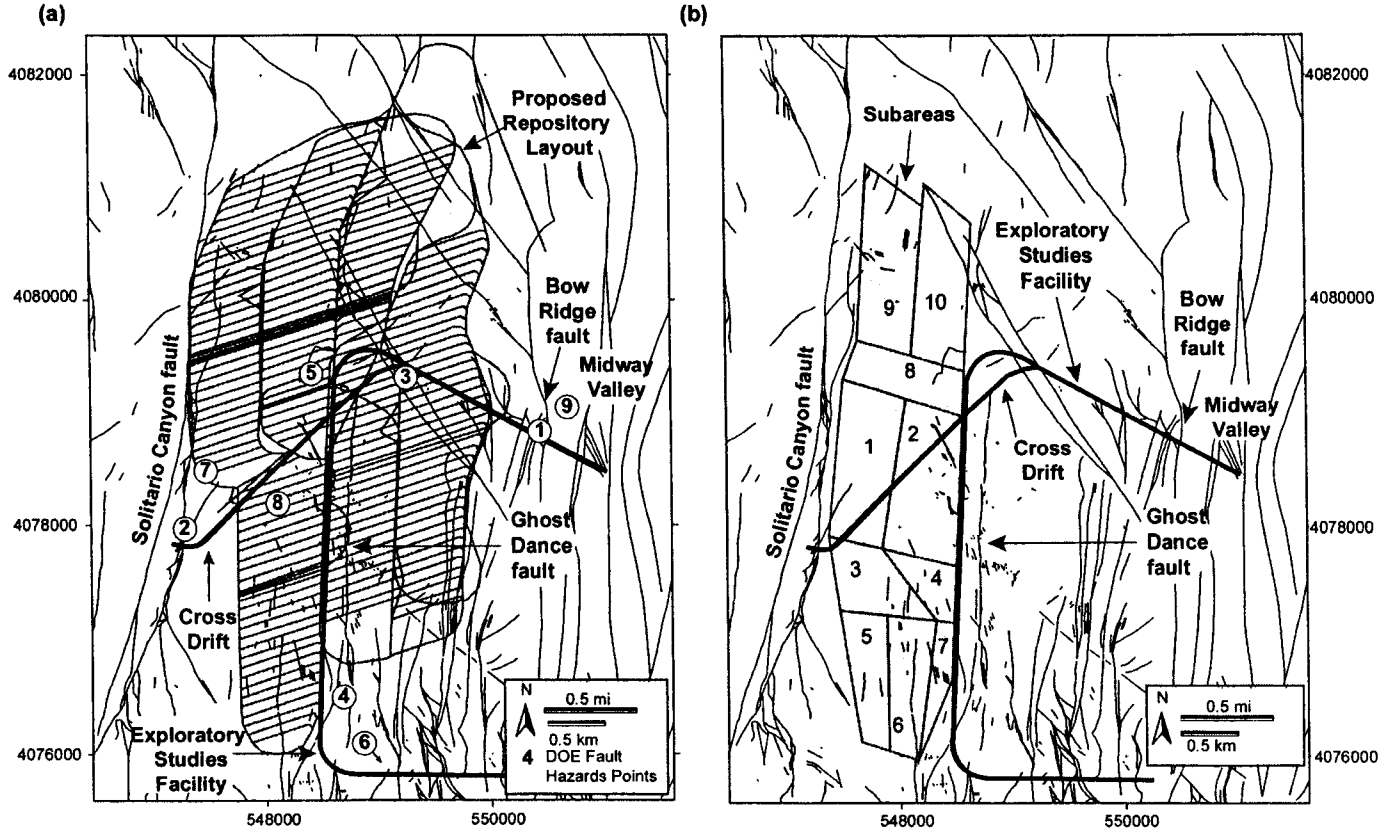

Figure 2-1. Maps Showing Proposed Repository Layouts Relative to Fault Traces Mapped at Yucca Mountain. Fault Traces Are from Day, et al. (1998a,b). The More Recently Proposed Repository Layout (CRWMS M&O, 2002) Is Shown in (a) As Are the Locations of the Nine Demonstration Points Used in CRWMS M&O (1998a). The Repository Layout with Subareas, As Defined in the NRC/CNWRA TPA Version 4.1j Code, Is Shown in (b). Coordinates Are in Universal Transverse Mercator (UTM) Zone 11, Using the North American Datum of 1927.

Table 2-1. Summary of the DOE Fault Displacement Results Demonstration Points for Fault Displacement Hazard Analyses

Point	Demonstration Point	Comment	Mean Fault Displacements (cm)		
			10^{-4}/yr	10^{-6}/yr	10^{-8}/yr
1	Bow Ridge Fault	Primary fault outside repository	< 1.0	52*	600†
2	Solitario Canyon Fault	Primary fault outside repository	< 1.0	180*	1400†
3	Drill Hole Wash Fault	Primary fault outside repository	< 1.0	14*	230*
4	Ghost Dance Fault	Secondary fault outside repository	< 1.0	15*	150*
5	Sundance Fault	Secondary fault within repository	< 1.0	6*	120*
6	Small Fault in Dune Wash	Secondary fault outside repository	< 1.0	12*	200*
7	100 m East of Solitario Canyon Fault	Within repository, four conditions assessed:			
		(a) small fault with 2-m displacement	< 1.0	4*	70*
		(b) shear with 10-cm displacement	< 1.0	1*	9.5*
		(c) fracture	< 1.0	< 1.0	< 1.0
		(d) intact rock	< 1.0	< 1.0	< 1.0
8	Center of Repository	Within repository, four conditions assessed:			
		(a) small fault with 2-m displacement	< 1.0	2*	80*
		(b) shear with 10-cm displacement	< 1.0	< 1.0	9*
		(c) fracture	< 1.0	< 1.0	< 0.1
		(d) intact rock	< 1.0	< 1.0	< 0.1

Table 2-1. Summary of the DOE Fault Displacement Results Demonstration Points for Fault Displacement Hazard Analyses (continued)

Point	Demonstration Point	Comment	Mean Fault Displacements (cm)		
			10^{-4}/yr	10^{-6}/yr	10^{-8}/yr
9	Midway Valley Fault	Outside repository footprint	< 1.0	11*	100†

* Derived from fault displacement hazard curves in CRWMS M&O (1998)
† Linear extrapolation of probabilistic fault displacement hazard curves in CRWMS M&O (1998)

CRWMS M&O. "Probabilistic Seismic Hazard Analyses for Fault Displacement and Vibratory Ground Motion at Yucca Mountain, Nevada." WBS 1.2.3.2.8.3.6. Oakland, California: DOE. 1998.

(ii) The probability of surface displacement was determined by the DOE expert teams in two ways: logistical regression of historical earthquake and surface displacement data from the Basin and Range (see Figure 4-11 of CRWMS M&O, 1998a) and focal depth calculations. In the focal depth calculations, the size and shape of the fault displacement for each earthquake were generally considered circular or elliptical (Figure 2-2). Displacements were then estimated from empirical scaling relationships (e.g., Wells and Coppersmith, 1994). Depending on focal depth, the potential surface displacement along the fault was determined. Because the maximum surface displacement may not coincide with the demonstration point, an additional variable that randomized the displacement along the fault length was also introduced. Thus, for both the historical earthquake and focal depth methods, the amount of surface displacement at the demonstration point for each event was determined based on the location of the demonstration point relative to the surface displacement (Figure 2-2).

(iii) The probability of secondary or distributed faulting was determined by the DOE experts in two ways: logistical best fit to data from Basin and Range historical displacements, in which the secondary or distributed faulting was mapped after an earthquake (U.S. Geological Survey, 1996), and slip tendency analysis (Morris, et al., 1996).

Results of the DOE probabilistic seismic hazard assessment (CRWMS M&O, 1998a) indicate that (e.g., except for the Bow Ridge fault, Solitario Canyon fault, and Midway Valley demonstration points), mean fault displacements are relatively small, even for mean annual exceedence probabilities of 10^{-8} (Table 2-1). For larger faults such as the Bow Ridge, Solitario Canyon, and Midway Valley faults, mean fault displacements that could impact the waste packages have exceedence probabilities of less than 10^{-4}/yr (Table 2-1).

Sensitivity analyses provided in the probabilistic seismic hazard assessment (CRWMS M&O, 1998a) show the earthquake and displacement methods produce similar hazard values. For example, the Ake, Slemmons, and McCalpin expert team generally estimated the greatest faulting hazard (i.e., largest displacement for 10^{-4}/yr) for each of the nine demonstration points.

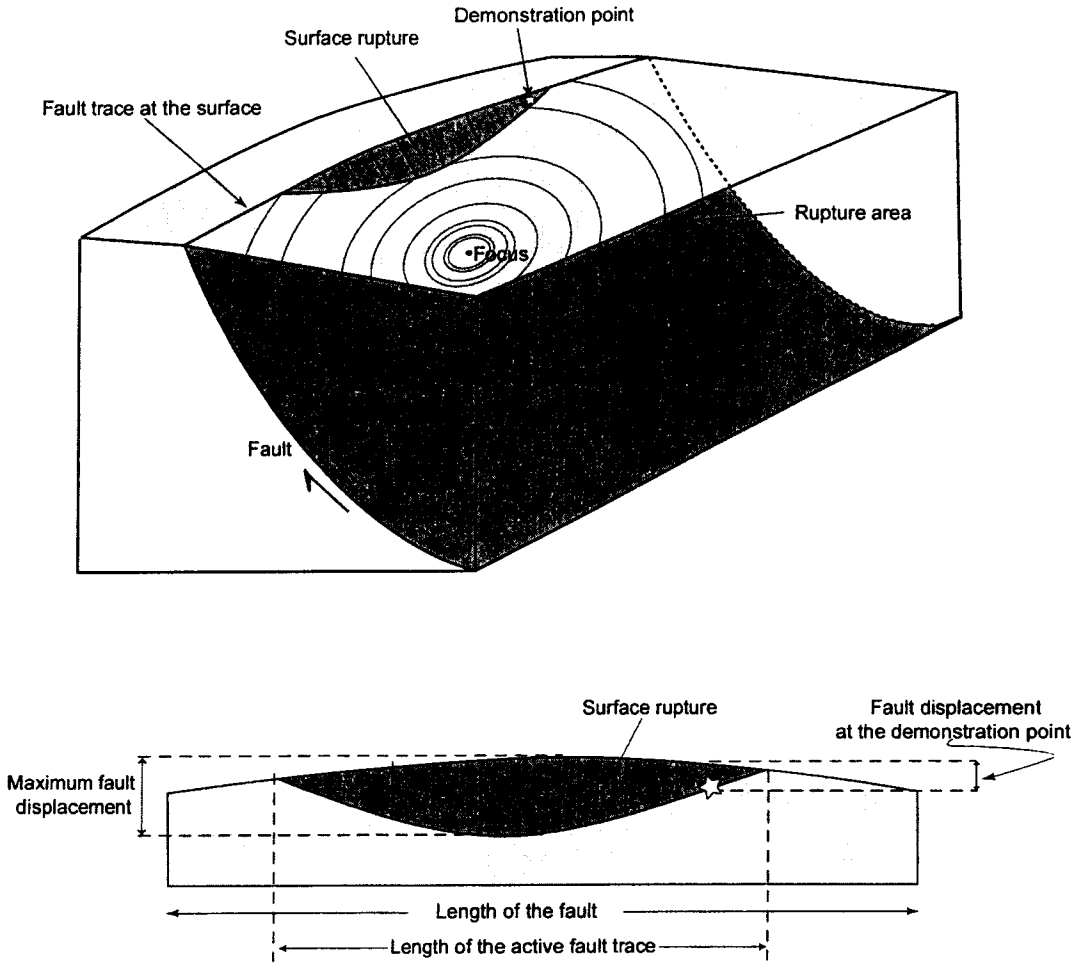

Figure 2-2. Illustration of an Idealized Fault Displacement Profile from an Earthquake. The Illustration Shows the Amount of Fault Displacement at a Demonstration Point Depends on Both the Maximum Fault Displacement and the Location of the Demonstration Point Along the Fault Surface Relative to the Maximum Displacement.

This team relied exclusively on the earthquake approach. The Smith, Bruhn, and Knuepfer expert team generally estimated the second greatest hazard using the displacement approach. Teams produced similar estimates of the hazard using both the earthquake and displacement approaches (CRWMS M&O, 1998a).

2.2 Staff Evaluation of the DOE Probabilistic Fault Displacement Hazard Assessment

Staff evaluated the DOE assumptions and results of the fault displacement hazard assessment provided in its probabilistic seismic hazard assessment (CRWMS M&O, 1998a) and concluded the DOE expert elicitation used a broad range of available data and technical interpretations in developing the probabilistic fault displacement hazard assessments. DOE has sufficient information for NRC to conduct a License Application review of the probability of faulting as it relates to postclosure repository performance (NRC, 1999, 2002a). Staff review of the probability of faulting included quality and completeness of the data and appropriate consideration of uncertainty. Further, staff evaluations (NRC, 1999, 2002a) included assessment of deterministic and probabilistic analyses of principal fault displacement, as well as integration of these analyses with structural and tectonic models used to assess secondary faulting.

2.3 The DOE Consequence Analyses of Fault Displacement

DOE considered the possible effects of faulting on postclosure repository performance through the CRWMS M&O (2000a) and three associated analyses and model reports (Table 2-2). Of the analyses and model reports, the first three listed in Table 2-2 are relevant to the Structural Deformation and Seismicity subissue of faulting. The Structural Deformation and Seismicity subissue of faulting only considers the probability and consequences of direct fault displacement of integral components of the subsurface engineered system, principally waste packages and drip shields. CRWMS M&O (2000b,c) and the first three analysis and model reports listed in Table 2-2 (CRWMS M&O, 2000d,e,f) form the basis for staff review.

Table 2-2. The DOE Analysis and Model Reports Supporting the Disruptive Events Process Models Report

Analysis and Model Report	ID Number	ID Number
Disruptive Events FEPs	T0010	ANL–WIS–MD–000005
Characterize Framework for Seismicity and Structural Deformation at Yucca Mountain, Nevada	T0075	ANL–CRW–GS–000003
Effects of Fault Displacement on Emplacement Drifts	T0115	ANL–EBS–GE–000004
Fault Displacement Effects on Transportation in the Unsaturated Zone	T0090	ANL–NBS–HS–000020

Based on the analyses summarized in the reports listed in Table 2-2, DOE concluded that faulting is too infrequent and fault displacements are too small to produce any direct fault displacement failures of the waste packages or drip shield (CRWMS M&O, 2000b). In addition, DOE concluded that fault displacements were too small on all but the Solitario Canyon fault to require fault setback in repository design (CRWMS M&O, 2000b).

The DOE analyses presented in the reports listed in Table 2-2, however, were based on the premise that median, rather than mean, values of fault displacement were appropriate to characterize fault displacements with exceedence probabilities less than 10^{-6} and as small as 10^{-8}. At these small exceedence probabilities, the median fault displacement values are significantly less than the mean values (c.f., mean versus median hazard curves in Figure 1-4). In addition, the DOE analyses assume that drift design will not include engineered backfill, and the drifts will remain stable without significant amounts of naturally occurring rockfall throughout the 10,000-year compliance period.

2.4 Staff Evaluation of the DOE Consequence Analyses of Fault Displacement

Staff evaluated the DOE assumptions and results of fault displacement consequence analyses provided in the reports listed in Table 2-2. Of primary concern in the analyses was whether the median fault displacement values were the appropriate statistic for use in risk-based consequence analyses or if the mean values should be used.[2] Based on the DOE response to the structural deformation and seismicity agreements reached with the NRC staff at a Technical Exchange held in October 2000, DOE will no longer use median values for fault displacements at low exceedence probabilities, but instead will use the mean values for all fault displacement analyses.[3] In addition, in recent discussion between the DOE and the Repository Design and Thermal-Mechanical Effects Key Technical Issue staffs, DOE is considering a significant change in the approach used to assess drift stability and rockfall. This new approach could lead to substantial changes in the DOE conclusions regarding rockfall, drift stability, and fault setback distances in repository design. Ongoing work by the staff and by DOE suggests that rockfall and drift degradation rates may be higher and more uncertain than previously indicated. Thus, future analyses of faulting hazard may need to consider the presence of fill in drifts.

Because of these three developments—(i) commitment to use mean fault displacement values, (ii) changes in the DOE approach to rockfall and drift stability analyses, and (iii) the potential for significant natural backfill in the drifts—conclusions reached by DOE in the reports listed in Table 2-2 need to be reevaluated. DOE agreed to reassess the potential consequences of faulting on postclosure performance (Stepp and Cornell, 2001). Given the DOE commitment in concert with the risk insights gained from the consequence analyses presented in this report, staff conclude that DOE will likely provide information on the potential consequences of faulting sufficient for NRC to conduct a License Application review if and when DOE submits a Licence Application to NRC.

---

[2] Schlueter, J.R. "U.S. Nuclear Regulatory Commission/U.S. Department of Energy Technical Exchange and Management Meeting on Structural Deformation and Seismicity (October 11–12)." Letter (October 27) to S. Brocoum, DOE. Washington, DC: NRC. 2000.

[3] Brocoum, S. "Transmittal of Report Addressing Key Technical Issues (KTI) Structural Deformation and Seismicity (SDS)." Letter (October 25) to C.W. Reamer, NRC. Washington, DC: DOE. 2001.

3 ASSESSMENT OF FAULTING USING THE NRC AND CNWRA TOTAL-SYSTEM PERFORMANCE ASSESSMENT CODE

3.1 FAULTO Methodology

3.1.1 Conceptual Model

The FAULTO module, which is part of the NRC/CNWRA TPA Version 4.1j code, evaluates the potential consequences associated with disruption of waste packages from fault displacements along single planar fault zones. In the TPA Version 4.1j code, displacement on a single fault is simulated as deformation within a tabular zone with finite thickness, herein defined as fault zone width. Within the simulated fault zone width, fault displacement and consequent deformation to waste packages are assumed uniform. Regions outside the fault zones are considered undeformed with no damage to waste packages. The number of damaged waste packages and location within the repository footprint are then used to estimate release of radionuclides and associated dose consequences.

In the most general application of the FAULTO module, a new fault is simulated to occur uniformly within the repository. Geometric characteristics of the simulated fault are derived from uncorrelated univariate probability distribution functions. These probability distribution functions define (i) location of the fault within the repository, (ii) azimuthal orientation of the fault zone, (iii) fault trace-length, and (iv) fault zone width. A complete list of the parameters sampled in the FAULTO module is provided in Table 2-4 of Ghosh, et al. (1997). In addition, the FAULTO module allows users to define two sets of faults, one set that trends northwest-southeast and one set that trends north northeast-south southwest. These two sets of faults are considered representative of a bimodal distribution of fault traces at Yucca Mountain. This bimodal distribution was based on fault data available prior to 1997, when the FAULTO module was first developed. Since then, a more complete inventory of fault data at Yucca Mountain has been compiled. These data now show that fault orientations span a single distribution of fault orientations that include both northwest-southeast and north northeast-south southwest trends (Figure 1-3b).

For the analytical methodology presented in this report, the general application of the FAULTO module was modified to specifically consider two simulated fault zones centered on the traces of the Ghost Dance and Solitario Canyon faults (Figure 1-3a and 1-3b). These two faults were chosen for this analysis as appropriate examples with which to evaluate faulting on intra-block secondary (i.e., Ghost Dance) and principal (i.e., Solitario Canyon) faults. The final repository layout and design for the drifts has not yet been finalized by DOE, including whether repository drifts will cross these or other faults or if DOE will include criteria for fault setback distances for emplacement of waste packages in its License Application.

Abstracting fault displacements for these two known faults, as opposed to an abstraction of randomly generated new faults in the repository, is supported by geological evidence at Yucca Mountain. Past faulting at Yucca Mountain is largely confined to faults that formed in the late Miocene during or shortly after major silicic caldera activity associated with the Southwest Nevada Volcanic Field. For example, stratigraphic and structural data, such as growth strata and cross-cutting relationships, indicate many faults at Yucca Mountain that formed since 10–12 Ma remain active to the present. Paleoseismic data from fault trenches across many of

the faults at Yucca Mountain also show evidence for repeated fault slip in the Quaternary (last 2 million years) on those early formed faults (U.S. Geological Survey, 1996). There is no geologic evidence at Yucca Mountain for fault displacements on the order of 20 to 500 cm [0.6 to 16.5 ft] (that could potentially impact the engineered systems) on geologically young faults (that formed in the last 1–2 millions of years). Based on these observations of the tectonic setting, staff consider future deformation at Yucca Mountain would likely reactivate existing faults, such as the Ghost Dance and Solitario Canyon faults, rather than cause new faults to form randomly within the repository.

Because the geometric characteristics of the Ghost Dance and Solitario Canyon faults are well established at the surface (Day, et al., 1998a,b; Simonds, et al., 1995) and in the Exploratory Studies Facility and Cross Drift (Mongano, et al., 1999), most of the geometric characteristics of these faults (i.e., location, length, azimuth, and dip) can be fixed to single values in the FAULTO module (Table 3-1).

3.1.2 Fault Zone Width

Calculated radiological dose may be sensitive to fault-zone width, which is the tabular zone of fault-induced deformation perpendicular to the fault displacement. Logically, wider fault zones incorporate more waste packages than discrete fault surfaces or narrow fault zones.

Table 3-1. Geometric Characteristics of the Solitario Canyon and Ghost Dance Faults

	Solitario Canyon Fault	Ghost Dance Fault
Parameter Description	**Distribution**	**Distribution**
Center of the Fault (UTM, Zone 11, North American Datum 27).	Constant Northing = 4078000 Easting = 547600	Constant Northing = 4078200 Easting = 548400
Strike (degrees)	Constant 005°	Constant 005°
Trace Length (m)	Constant 6000	Constant 6000
Width (m) 0.1 percentile 99.9 percentile	Lognormal $p_{0.001}$ = 0.294 $p_{0.999}$ = 339.5	Lognormal $p_{0.001}$ = 0.0116 $p_{0.999}$ = 62.8

NOTE: Information provided in meters; for conversion, use 0.31 m = 1 ft.

Fault-zone width is an uncertain geometric parameter. Based on detailed geologic maps of surface (Day, et al., 1998a,b) and subsurface exposures (Mongano, et al., 1999), fault-zone width varies along the strike and dip of both faults. Fault-zone width also can vary from one fault to the next. To model fault-zone width in the TPA Version 4.1j code, probability distribution functions were created from fault and fracture data acquired in the Exploratory Studies Facility, where the Bureau of Reclamation mapped 826 fault surfaces, 115 of them with thicknesses greater than 1 cm [0.16 ft] (Mongano, et al., 1999). The measured widths of these 115 faults describe a lognormal distribution (Figure 3-1a). In the absence of more definitive information about the future kinematic behavior of fault slip within the Ghost Dance and Solitario Canyon fault zones, these lognormal distributions are assumed to represent fault-zone widths sampled in the FAULTO module and TPA Version 4.1j code analyses (Table 3-1).

Because the Ghost Dance fault appears to be part of a continuum of secondary intra-block faults within the proposed Yucca Mountain repository footprint (Figures 1-3b, 2-1a, and 2-1b), a probability distribution function was derived for fault-zone width of the Ghost Dance fault that matched the measured fault widths in the Exploratory Studies Facility (c.f., Figure 3-1a to Figure 3-1b). For the Solitario Canyon fault, a similar lognormal distribution shape was used (Figure 3-1c). Because the Solitario Canyon fault is a block-bounding fault, the mean value and standard deviation of the probability distribution function were adjusted to reflect substantially larger fault-zone widths, similar to fault-zone widths of the Solitario Canyon observed in the Cross Drift (Mongano, et al., 1999).

3.1.3 Faulting Recurrence

In addition to geometric characteristics of faults, the general application of the FAULTO module also allows the user to establish probability distribution functions to model parameters related to the likelihood of faulting and the likelihood of a given amount of fault displacement during a faulting event. These parameters are (i) displacement per faulting event, (ii) recurrence interval of faulting, and (iii) fault displacement rate. The values from these probability distribution functions, along with an established threshold for the minimum amount of displacement necessary to cause waste package damage, are used to evaluate potential failures of the waste package.

Direct sampling of the likelihood parameters for a faulting event is impractical for the TPA Version 4.1j code calculations. The exceedence probabilities of consequential fault displacements that could potentially impact the engineered systems at Yucca Mountain are estimated to be less than 10^{-4}/yr based on the DOE probabilistic fault displacement hazard results (CWRMS M&O, 1998a). This low-probability event would require at least 10^{6} realizations of the TPA Version 4.1j code to get an adequate stochastic sample. Thus, consequences of faulting were evaluated by including a faulting event in each TPA Version 4.1j code realization that damaged waste packages and caused radiological release. The resulting conditional doses were then weighed by the annual probability of the faulting event. As discussed in the following section, the probability used to weight the conditional doses depends on what is determined to be an appropriate amount of threshold fault displacement.

3.1.4 Threshold Fault Displacements for Waste Package Failure

The probability that a given faulting event produces sufficient fault displacement to cause waste package failure was derived directly from the DOE probabilistic fault displacement hazard

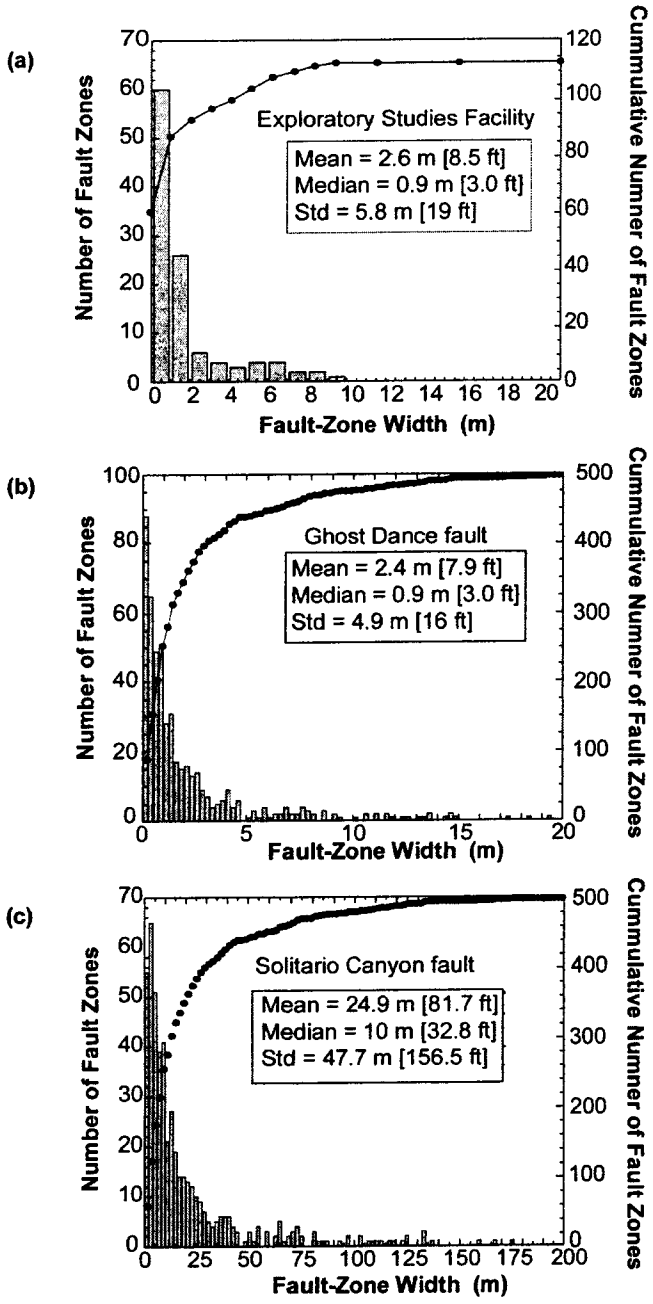

Figure 3-1. Histograms and Cumulative Frequency Curves Showing Probability Distribution Functions for Fault Widths Used in Total System Performance Assessment Calculations. Fault Width Distribution (a) from Fault and Fractures Mapped in the Exploratory Studies Facility Based on Data from Mongano, et al. (1999). Fault Width Distributions Developed in This Report for the Ghost Dance (b) and Solitario Canyon (c) Faults. The Ghost Dance and Solitario Canyon Faults Results Are from 500 Realizations of the FAULTO Module within the NRC/CNWRA TPA Version 4.1j Code.

results (Table 2-1, Figure 1-4) along with upper-bound estimates of the minimum amount of fault displacement necessary to impinge a waste package within repository drifts. The threshold fault displacement necessary to impinge a waste package within the drifts depends in large part on whether the drifts are backfilled or remain open during the postclosure period. In an open drift, current design (CRWMS M&O, 2002) shows the minimum clearance between the waste packages and drift walls is more than 1 m [3.2 ft] and occurs between the side wall of the drift and the base of the waste package–drip shield configuration. Thus, for open drifts, 1 m [3.2 ft] of fault displacement is deemed the minimum threshold for fault displacement that could cause the waste packages to lose their ability to contain radionuclides.

If the drifts are backfilled, whether by design or from progressive drift degradation, then the threshold displacement that could lead to waste package failure is less than the 1 m [3.2 ft] threshold for open drifts. For a completely filled drift in which the waste packages or drip shields are covered by debris, even a small fault displacement could impact the waste packages, assuming minimal compaction or rock debris in the drift. This assumption is especially true for the planned defense high-level waste packages, which have an approximately 20 cm [0.67 ft] clearance to the struts supporting the drip shields (CRWMS M&O, 2002). Thus, 20 cm [0.67 ft] was selected as the minimum threshold displacement that could lead to waste package failure for backfilled drifts.

The annual exceedence probabilities for 1 m [3.2 ft] and 0.20 m [0.64 ft] of fault displacement on the Ghost Dance and Solitario Canyon faults are shown in Table 3-2. These values were extrapolated from the DOE probabilistic fault displacement hazard curves (CRWMS M&O, 1998a).

Table 3-2. Annual Exceedence Probabilities for the Ghost Dance and Solitario Canyon Faults for 1 m [3.2 ft] and 0.2 m [0.64 ft] Fault Displacements

Fault	Statistical Measure	Annual Exceedence Probability	
		1.0 m [3.2 ft]	0.2 m [0.64 ft]
Solitario Canyon	85th percentile	6×10^{-6}	2×10^{-5}
	Mean	3×10^{-6}	2×10^{-5}
	Median	9×10^{-7}	6×10^{-5}
	15th percentile	3×10^{-8}	4×10^{-6}
Ghost Dance	85th percentile	4×10^{-8}	6×10^{-7}
	Mean	3×10^{-8}	1×10^{-7}
	Median	$< 1 \times 10^{-8}$	3×10^{-7}
	15th percentile	$< 1 \times 10^{-8}$	$< 1 \times 10^{-8}$

The criteria used to estimate and model waste package failure in this methodology are based on highly simplistic and pessimistic assumptions about the mechanical response of waste packages during faulting. Detailed mechanistic response models of the waste packages under the types of physical loads induced by faulting have not been developed. To overcome this limitation, all waste packages within a sampled fault-zone width were assumed to be impacted by a simulated fault displacement above the threshold displacement. Once the waste packages are impinged within the drifts, they are assumed to fail in a way that cause immediate contact of the waste with any water flowing into the drift. Thus, for each TPA Version 4.1j code faulting realization, every waste package within the simulated fault zone was assumed to fail and to expose the contents to the groundwater pathway. Consistent with this assumption, the flow-through option in the EBSREL module of the TPA Version 4.1j code was used. As with other noted conservatisms, this simplistic model for waste package failure from faulting was adopted to develop an ostensibly conservative evaluation of the consequences of faulting. In the event this approach showed that faulting could make a significant contribution to overall repository risk, the mechanical behavior of waste packages under faulting loads would need to be refined to capture greater realism and reduce undue conservatism.

This simplistic approach provides a method to work around for a limitation in the TPA Version 4.1j code, which does not have an explicit link between waste package and drip shield failure. In the TPA Version 4.1j code, drip shields remain unaffected by simulated faulting events, even if a faulting event disrupts the waste packages directly below the drip shields. To overcome this limitation, the beneficial effects of the drip shields were removed by setting the drip shield failure time in the EBSFAIL module to 0 years and the drip shield thickness to 0.001 m [0.003 ft] in the NFENV module. As before, if this approach showed that faulting could make a significant contribution to overall repository risk, the mechanical behavior of the drip shields and their link to deformation of the waste packages under faulting loads would need to be refined to capture greater realism and reduce undue conservatism.

3.2 Conditional Dose Estimates

To estimate conditional dose from potential faulting events, a series of TPA Version 4.1j code runs was completed for both the Solitario Canyon and Ghost Dance fault examples. Each run used 500 realizations to ensure statistically reliable results. Except for the parameters modified within the FAULTO, EBSFAIL, and NFENV modules discussed in Section 3.1, the full range of parameter variability in the standard basecase input file was used. In the analyses performed for this report, and for reasons discussed in the succeeding sections on risk, TPA Version 4.1j code runs were made for faulting events initiated at years 100; 2,000; and 4,000. A run was also made assuming a uniform distribution of faulting throughout the 10,000-year compliance period.

Results of conditional dose versus time for postclosure faulting events on the Ghost Dance and Solitario Canyon faults that were forced to occur at year 100 are shown in Figure 3-2. The curves summarize the runs showing maximum and minimum values, as well as the mean, median, and 95th percentile. All the curves show an initial peak in calculated conditional dose within approximately 2,000 years of the faulting event, indicating the influence of the thermal pulse on the initial solubility rates of radionuclides. The curves also show a steady increase in conditional dose versus time reaching a second maximum at year 10,000. The analyses performed for this report did not examine conditional dose beyond year 10,000.

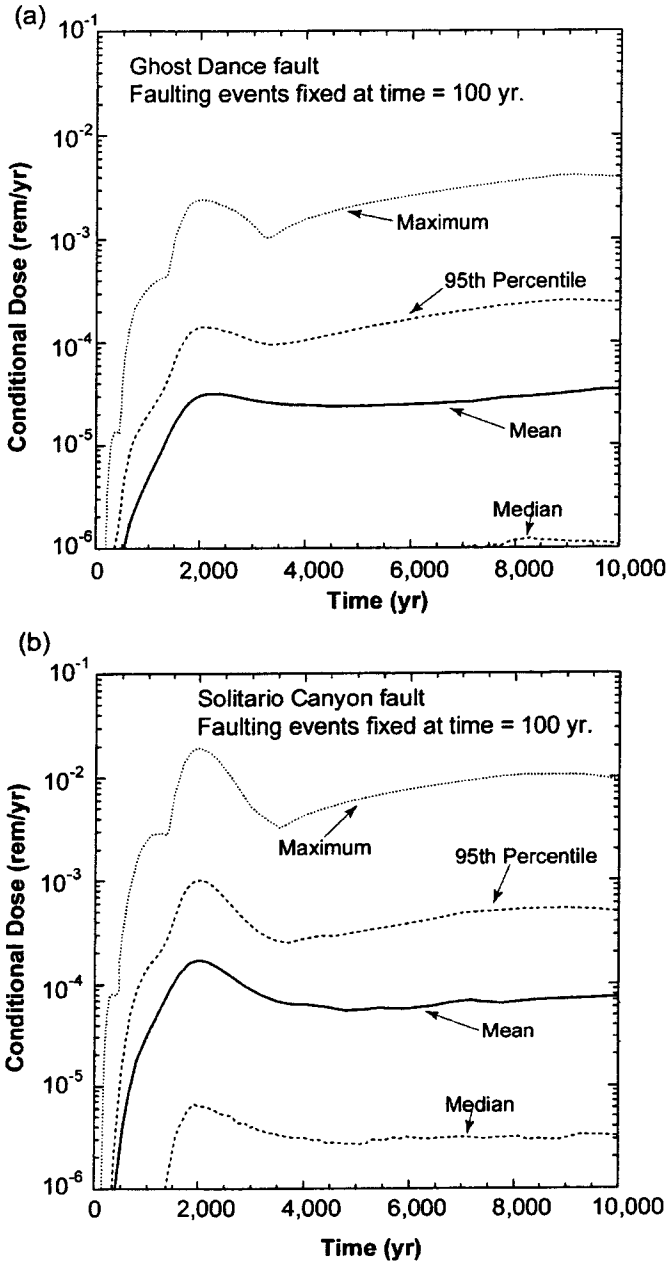

Figure 3-2. Graphical Plots of the Conditional Doses Through Time in Which Faulting Events Are Forced to Occur at Postclosure Year 100. Results Are Presented for the Ghost Dance (a) and Solitario Canyon (b) Faults. The Plots Present the Mean, Median, 95th Percentile, and Maximum Values of 500 Realizations. In These Calculations, All Waste Packages That Fall Within the Zone of Deformation Around the Named Fault Are Assumed to Fail and to Permit Release of Radionuclides.

Dose versus time curves for the TPA Version 4.1j code runs on the Solitario Canyon fault, in which faulting was forced to occur in years 2,000 and 4,000, and one run in which faulting events occur uniformly throughout the 10,000 year compliance period, are compared to the 100-year results in Figure 3-3. As expected, results show that conditional doses are lower for faulting events that occur farther into the future, especially when the faulting events are uniformly distributed in the 10,000-year compliance period. In addition, faulting events that occur after the thermal pulse do not show the initial peak in conditional dose that is prominent in the 100-year curves. This observation is consistent with the interpretation that the thermal pulse strongly contributes to early solubility-driven releases in the 100-year faulting curves.

3.3 Risk from Faulting

3.3.1 Risk Calculation Procedure

The final step in this application of the FAULTO module is to formulate the results for risk. Risk is obtained by multiplying the calculated conditional doses by the probability that a fault displacement could lead to waste package failure and release of radionuclides.

In a complete computation of the risk, risk from faulting in any given year includes the risk from events occurring in that year plus the cumulative risk of faulting events in all previous years. Because of time sensitive input to the release of radionuclides and groundwater transport, the risk from faulting will vary from year to year. Thus, a complete calculation of annual risk would require realizations for faulting events in each year between year 100 (i.e., the end of the preclosure period) through year 10,000. Risk could then be summed, year by year, to estimate the overall risk in the year of interest. For example, the risk due to faulting in year 5,000 is the probability-weighted dose from a faulting event in that year plus the years back to year 100. Given 250–500 realizations per run necessary for a stable mean dose, a complete risk calculation to year 10,000 would require 9,900 TPA Version 4.1j code runs and 3,465,000–4,950,000 realizations (250–500 × 9,900).

To simplify the risk calculations, the dose consequences for a faulting event that occurs at year 100 was used to bound faulting-related dose consequences for faulting events in any subsequent year. This simplifying assumption is conservative in that the doses from the 100-year faulting event are demonstratively larger (e.g., Figure 3-3) than for a faulting event in any subsequent year. This simplifying assumption is supported by the following list of features of the radioactive waste, engineered systems, and natural barriers at Yucca Mountain.

(i) Following waste package failure, release of radionuclides to the accessible environment and into the groundwater at the compliance boundary is by groundwater flow through the unsaturated zone underneath the repository horizon and the saturated zone from the repository and down hydrologic gradient to the compliance boundary.

(ii) Because the release is through groundwater, the soluble radionuclides are the important contributors to dose: I-129, Tc-99, and Np-237 (Mohanty, et al., 2002a).

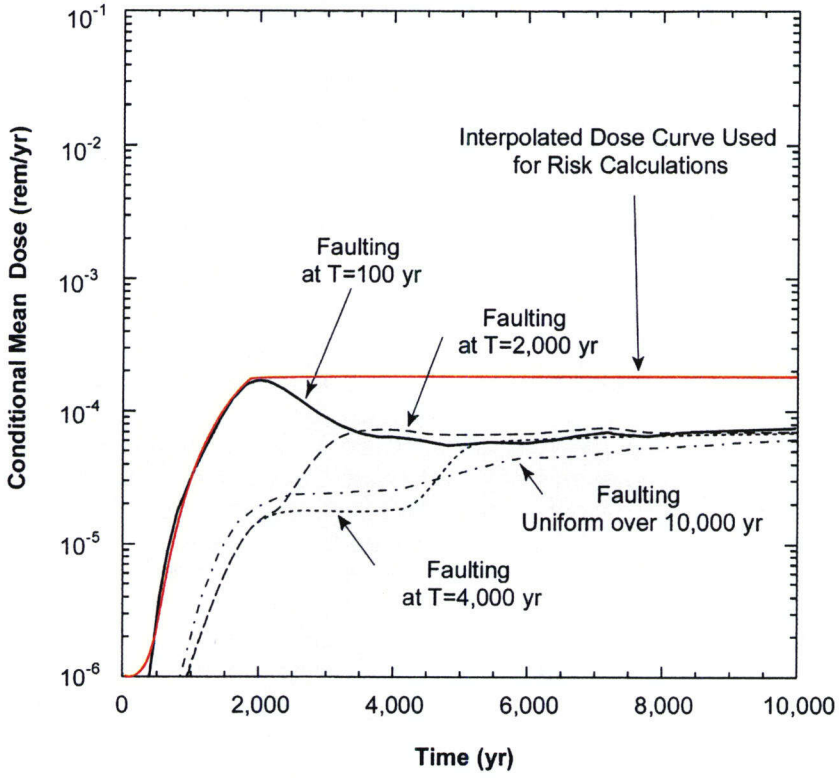

Figure 3-3. Comparison of the Mean Dose Versus Time Curves for Cases in Which the Faulting Events on the Solitario Canyon Fault Were Forced to Occur in All 500 Realizations at a Specified Year (100, 2,000, and 4,000) and for a Case in Which the Faulting Events Occurred Uniformly over the Entire 10,000 Year Postclosure Period. The Red Line Shows the Interpreted Dose Versus Time Curve Used in the Risk Calculations.

(iii) Doses from I-129, Tc-99, and Np-237 depend primarily on amount of water entering the drifts, dissolution rates of the spent nuclear fuel, radionuclide solubility, groundwater travel times, sorption, matrix diffusion, fracture porosity, and dispersion (Mohanty, et al., 2002a). The time it takes to fill the damaged waste packages with water is not a factor in these calculations because a flow-through failure mode was used.

(iv) All the factors listed in (iii) lead to delay in the release of radionuclides from the damaged waste packages. For example, Mohanty, et al. (2002a) report that the combined travel times for these radionuclides in the unsaturated and saturated zones varied between 589 and 1,395 years, with a repository average of 926 years. Solubility limits and fuel dissolution may also delay release by a similar amount. The mean dose versus time curves in Figure 3-2a and 3-2b show the peak dose occurs just after year 2,000, consistent with the expected 1,000–2,000 year lag times following waste package damage because of groundwater travel times, waste decay, and solubility limits.

(v) For waste package failures that might occur significantly after year 100, doses will likely be smaller and lag times longer, mainly because solubility limits for these radionuclides are lower after the thermal pulse concludes.

(vi) A slight reduction in inventory occurs between years 100 and 10,000. Half-lives for I-129, Tc-99, and Np-237 range between 10^5 and 10^7 years (Mohanty, et al., 2002a).

As a test of the assumption that the 100-year faulting event is bounding, the mean conditional dose versus time curves for faulting events on the Solitario Canyon fault at years 2,000 and 4,000 are compared to the conditional dose versus time curve for the 100-year faulting event in Figure 3-3. Also shown in Figure 3-3 is the conditional dose versus time curve in which the faulting events occur uniformly throughout 10,000 years. In these TPA Version 4.1j code calculations, the 100-year faulting runs on the Solitario Canyon fault produce the largest conditional peak mean dose (1.660×10^{-4} rem). This conditional mean peak dose occurs at year 2,043. The conditional mean peak doses for all other cases are less than 1.0×10^{-4} rem.

In the risk calculations for faults, the 100-year conditional dose versus time curves was used to develop the peak doses for each year from postclosure year 100 to year 10,000. Conditional doses for each year were calculated using an interpolated best fit polynomial function to the 100-year dose versus time curve between years 100 and 2,000. For all years thereafter, the maximum conditional peak mean dose was used as a constant value equal to the year 2,000 dose. The conditional mean dose (D_c) at time (t) between years 100 and 2000 is given by

$$D_c = A_0 + A_1 t + A_2 t^2 + A_3 t^3 + A_4 t^4 \qquad (3\text{-}1)$$

where t is time and A_0 to A_4 are coefficients given in Table 3-3.

Table 3-3. Best-Fit Dose Versus Time Coefficients			
Fault	**Year of Maximum Conditional Mean Peak Dose**	**Maximum Conditional Mean Peak Dose (rem)**	**Best-Fit Polynomial Coefficients**
Solitario Canyon	2,043	1.7×10^{-4}	$A_0 = -1.27 \times 10^{-6}$ $A_1 = 2.42 \times 10^{-8}$ $A_2 = -9.13 \times 10^{-11}$ $A_3 = 1.35 \times 10^{-14}$ $A_4 = -3.681 \times 10^{-17}$
Ghost Dance	2,251	3.2×10^{-5}	$A_0 = -1.9 \times 10^{-6}$ $A_1 = 1.58 \times 10^{-8}$ $A_2 = -3.63 \times 10^{-11}$ $A_3 = 3.61 \times 10^{-14}$ $A_4 = -8.94 \times 10^{-18}$

3.3.2 Estimates of Risk

This interpolated dose versus time curve bounds all the other dose versus time curves (Figures 3-3 and 3-4) and, therefore, provides a reasonable upper bound on the risk estimated for faulting. As noted in Section 1.2, this approach was taken because the intent in this evaluation was to scope the potential risks from faulting and thereby gain risk insights about this disruptive event. If this approach shows that faulting makes a significant contribution to overall repository risk, the faulting performance assessment methodologies developed in this report will need to be refined to capture greater realism.

From the interpolated conditional dose versus time curve, the probability-weighted doses for each year between years 100 and 10,000 were then calculated. This was accomplished using the mean annual exceedence probabilities for both 0.20-m- [0.67-ft]- and 1.0-m- [3.2-ft]-threshold fault displacements, which were assumed for the backfilled and nonbackfilled scenarios, respectively (see Section 3.1.2 and Table 3-2). Risk in each year was then computed by summing the risks for all events occurring in prior years. Peak risk occurred in year 10,000 for each fault displacement scenario (Table 3-4).

Table 3-4. Risk Estimates for Faulting on the Solitario Canyon and Ghost Dance Faults		
Fault	**Mean Risk at Year 10,000 Assuming 0.20 m [0.67 ft] Threshold Fault Displacement (rem)**	**Mean Risk at Year 10,000 Assuming 1.0 m [3.2 ft] Threshold Fault Displacement (rem)**
Solitario Canyon	3.1×10^{-5}	4.6×10^{-6}
Ghost Dance	2.7×10^{-8}	8.2×10^{-9}

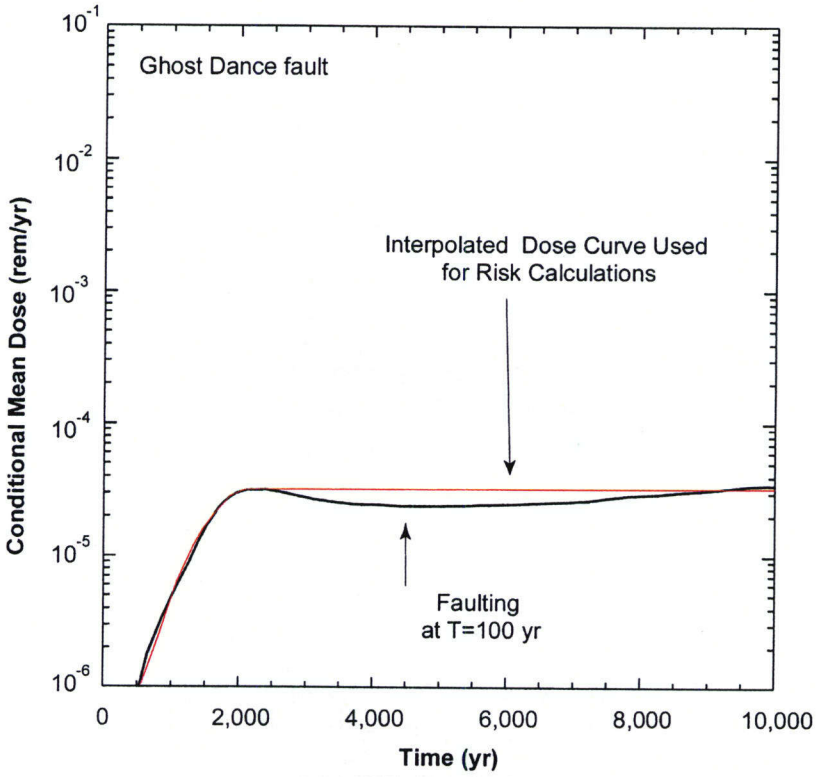

Figure 3-4. Comparison of the Conditional Mean Dose Versus Time Curve for Faulting Events on the Ghost Dance Fault That Are Forced to Occur in All 500 Realizations at Year 100, Compared to the Interpreted Dose Versus Time Curve Used in the Risk Calculations

3.3.3 Risk Insights

As noted in the preceding sections, these risk estimates are derived from numerous highly conservative or pessimistic assumptions about the mechanical behavior of waste packages and the characteristics of faulting at Yucca Mountain. For example

- No credit was taken for the benefits of the drip shields. Limitations in the TPA Version 4.1j code do not allow for a direct link between faulted waste package and over-capping drip shields. In the analyses in this report, the drip shields were removed from the engineered system.

- A flow-through model was used to simulate water entering into and exiting from damaged waste packages. This model implies that all waste packages are breached in such a way that water can enter and exit immediately after fault slip.

- Failure of the waste packages was assumed once a threshold displacement was reached, and the waste packages were in contact with the drift walls or drift fill. No credit was taken for the material strength or ductility of the waste package material.

- The threshold displacements of 1 m [3.2 ft] or 0.20 m [0.67 ft] are based on the minimum clearance between waste package and the drifts walls for end-member cases in which the drifts remain open or are backfilled.

- All waste packages located within the fault-zone widths are assumed to fail, even for wide fault zones.

- To simplify the risk calculation, the risk due to faulting in any year was based on an extrapolation of the mean condition dose versus time curve for a faulting event at year 100. This extrapolated curve yields larger conditional doses than would occur if actual dose calculations were performed in appropriate postclosure years.

Despite these conservative and pessimistic assumptions, risks due to direct rapture of waste package due to faulting on postclosure repository performance appear small, on the order of pico-rem to tens of micro-rem doses per year (Table 3-4). Low risks from faulting arise from the relatively small annual exceedence probabilities for consequential fault displacements at Yucca Mountain (Table 3-2) and the relatively few waste packages incorporated in fault zones. The relatively small risks of faulting, therefore, support the DOE conclusion that direct faulting of the drifts and waste packages is a disruptive event process that can be screened from a total system performance assessment based on low risk significance relative to the current understanding of Yucca Mountain total system performance.

3.4 Limitations to FAULTO Methodology

As summarized previously, the current abstraction of faulting in the FAULTO module inaccurately portrays the distributed nature of faulting, both within fault zones and the relationship to larger fault displacements on nearby principal faults. Faults in the FAULTO module are simply represented as single tabular zones of deformation, within which the displacement and consequent deformation are treated as a uniform process (Figure 3-5a). No deformation is considered to occur outside these discrete fault zones.

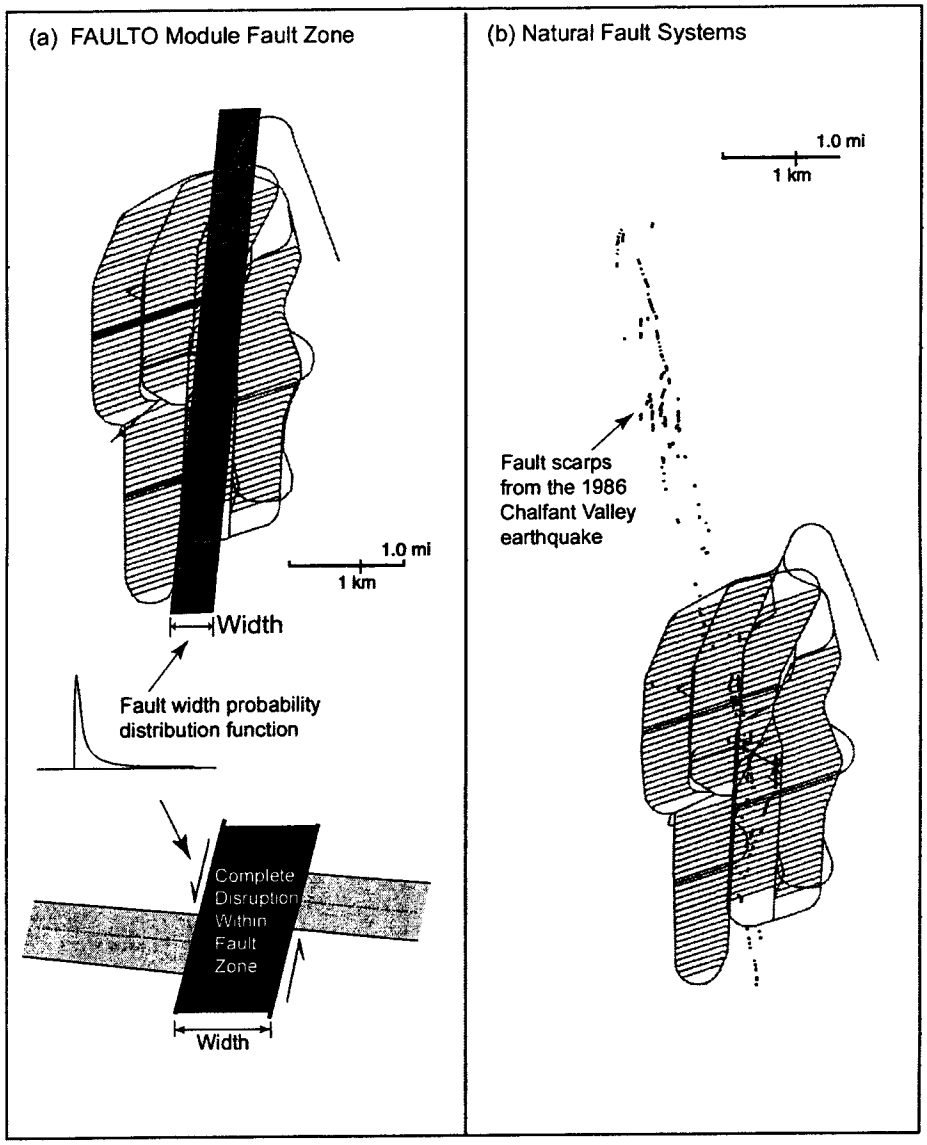

Figure 3-5. Schematic Illustrations That Compare the Way in Which Fault Zones Are Modeled on the FAULTO Module to a More Realistic Conceptual Model of Faulting. The Map Inset in (a) Shows the Repository Layout with a Modeled Fault Zone. The Black Box on the Cross Section in (a) Shows the Region Where Waste Packages Are Disrupted in the Fault Zone. Fault Widths in (a) Are Sampled in the FAULTO Module from a Lognormal Probability Distribution Function. The Map Inset in (b) Shows the Repository Layout Overlain on a Portion of the Map of Fault Scarps from the 1986 Chalfant Valley Earthquake (Cockerham and Corbett, 1987; Lienkaemper, et al., 1987; Smith and Priestley, 2000) Drawn at the Same Scale.

In contrast, observations from historical earthquakes show the spatial distributions of surface faulting associated with moderate- to large-magnitude earthquakes are complex (Figure 3-5b). Faulting often is discontinuous along individual fault segments of the principal fault and distributed on numerous secondary fault strands covering a large area around the principal fault (de Polo, et al., 1991).

Several observations of faults and faulting at Yucca Mountain support this characterization of faulting as a complex pattern of displacement surfaces and fault-induced damage zones. First, actual fault-zone widths at Yucca Mountain cannot be unambiguously defined. In some cases, fault-related deformation is confined to a discrete fault surface clearly identifiable compared with adjacent undeformed host rock. In other cases, however, a fault zone consists of one or more fault strands surrounded by a diffuse and wide zone of fractures or brecciated rock that grades laterally into undeformed host rock. For example, the 13–20 m [4–66 ft] of cumulative throw on the Ghost Dance fault at Antler Ridge is partitioned on several fault splays distributed over a 100–150-m- [30–490-ft]-wide fault zone (Day, et al., 1998a). Ghost Dance exposures on the USW UZ–7a drill pad consist of two clearly identifiable near-vertical fault splays that separate 42 m [138 ft] of intensely fractured and broken bedrock (Day, et al., 1998a). Similarly, the width of the Solitario Canyon fault also varies along strike at the surface near Yucca Mountain, from narrow and discrete fault traces to fault zones as much as 400 m [1,312 ft] wide, within which lenses and blocks of Tiva Canyon and Topopah Spring tuffs are juxtaposed (Day, et al., 1998a).

The wide surface exposures of the Ghost Dance and Solitario Canyon fault zones contrast with the much narrower exposures of these faults in the Exploratory Studies Facility and Cross Drift. In the subsurface, measured widths of the Ghost Dance fault are 2.5–10 m [8–33 ft] (Mongano, et al., 1999). In the Cross Drift, the eastern splay of the Solitario Canyon fault was exposed by the tunnel boring machine, but tunneling ceased before the western splay was encountered. In the subsurface, the eastern splay is composed of a discrete band of well-developed foliated fault gouge surrounded by a wide area of brecciated deformation (Gray, et al., 1998). Similar to the surface exposure, lenses of Tiva Canyon and Topopah Tuffs are tectonically mixed in the hanging wall exposed in the Cross Drift. Footwall deformation is also conspicuous, characterized by a wide zone of variably faulted breccia extending approximately 50 m [164 ft] east of the fault gouge. Mongano, et al. (1999) note, however, that this zone of footwall deformation may instead be related to an intersecting fault splay.

Mapped fault-zone widths at Yucca Mountain were produced by repeated fault slip events as a result of the many earthquakes that occurred in the region over the past 11 million years. The portion of the fault zone that is actually deformed by any single faulting event is unknown. The presence of a well-developed foliated fault gouge, which is mechanically weaker than the surrounding fractured Tuff, suggests that fault slip has been progressively isolated within the Solitario Canyon fault gouge. In this interpretation, future fault slip on the Solitario Canyon fault likely would be restricted to the rather narrow fault core (Gray, et al., 1998). Alternatively, recemented fault breccia within the Ghost Dance fault zone may, in places, be mechanically stiffer than the adjacent and unfaulted wall rock. Future slip could then occur at the margins of the Ghost Dance fault, causing the fault zone to widen with time (Gray, et al., 1998).

Because of these limitations in the abstraction of faulting in the FAULTO module, an alternative approach was developed for staff to evaluate the risk significance of faulting. This alternative approach is described in Chapter 4.

4 ASSESSMENT OF FAULTING USING FAULT DISPLACEMENT ANALOGS FROM HISTORIC EARTHQUAKES

4.1 Analog Faulting Methodology

As an alternative to the abstraction of faulting in the FAULTO module of the TPA Version 4.1j code, an alternative methodology has been developed based on fault displacement pattens from historic earthquakes in the Basin and Range Province. Processes of fault deformation produced by these earthquakes are considered analogous to deformation at Yucca Mountain. By analogy with historic earthquake activity in the western United States, large magnitude seismic slip on a fault at Yucca Mountain is likely to generate fault displacements in the vicinity of the epicenter of the main shock (Tocher, 1956; U.S. Geological Survey, 1964; Bell, 1984; Barrientos, et al., 1987; Crone, et al., 1987; Hanks and Schwartz, 1987; Lienkaemper, et al., 1987; dePolo, et al., 1991; Wells and Coppersmith, 1994; Hill and Bartholomew, 1999). Displacements of this type have offset magnitudes ranging from <0.1 to >4 m [<0.33 to >13.12 ft] (Lienkaemper, et al., 1987; dePolo, et al., 1991). These displacements often exceed the damage threshold in the TPA Version 4.1j code, suggesting potential faulting damage to the waste packages and drip shields.

4.1.1 Historical Faulting in the Basin and Range As an Analog to Faulting at Yucca Mountain

For this methodology, four historic earthquakes that produced surface displacements were selected as analogs to faulting at Yucca Mountain (Figure 4-1): (i) 1986 Chalfant Valley earthquake, (ii) 1983 Borah Peak earthquake, (iii) 1954 Rainbow Mountain–Stillwater earthquakes, and (iv) 1959 Hebgen Lake earthquake. All these earthquakes occurred within the western United States. The surface displacement patterns (both primary and secondary faulting) for these historical earthquakes are well documented. Faulting characteristics of these four displacement analogs are similar to those observed at Yucca Mountain. Fault displacements of the four analog events were predominantly the result of extensional strains, resulting in normal dip slip, with occasional strike slip, and few reverse slip displacements. Similar to maximum earthquake magnitudes and fault displacements predicted for principal faults at Yucca Mountain (CRWMS M&O, 1998a), the magnitudes of the four analog earthquakes ranged between 6.2 and 7.5, with measured maximum vertical offset (throw) 0.111 to 4.6 m [0.36 to 15.1 ft]. The surface trace lengths of the four analog faults ranged in length from 13.2 to 52 km [8.2 to 32.3 mi], which are also comparable to trace lengths observed at Yucca Mountain (e.g., Simonds, et al., 1995).

4.1.1.1 Chalfant Valley

The 1986 Chalfant Valley earthquake ($\mathbf{M_S}$ = 6.2) occurred in the White Mountains Frontal Fault Zone along the eastern edge of northern Owens Valley, California (Cockerham and Corbett, 1987; Lienkaemper, et al., 1987; Smith and Priestley, 2000) (Figure 4-1). Focal mechanism depth was 11.5 km [7.2 mi], with a strike of 335° and a southwest dip of 60°. Displacement along the 13.2-km- [8.2-mi]-long main displacement was predominantly right-lateral strike slip. Maximum right-lateral offset of 0.111 m [0.364 ft] across the main displacement fault system was toward the north end, with slip decreasing southward. Associated hanging wall extensional faulting occurred in the Volcanic Tablelands as six left-stepping *en echelon* fracture zones.

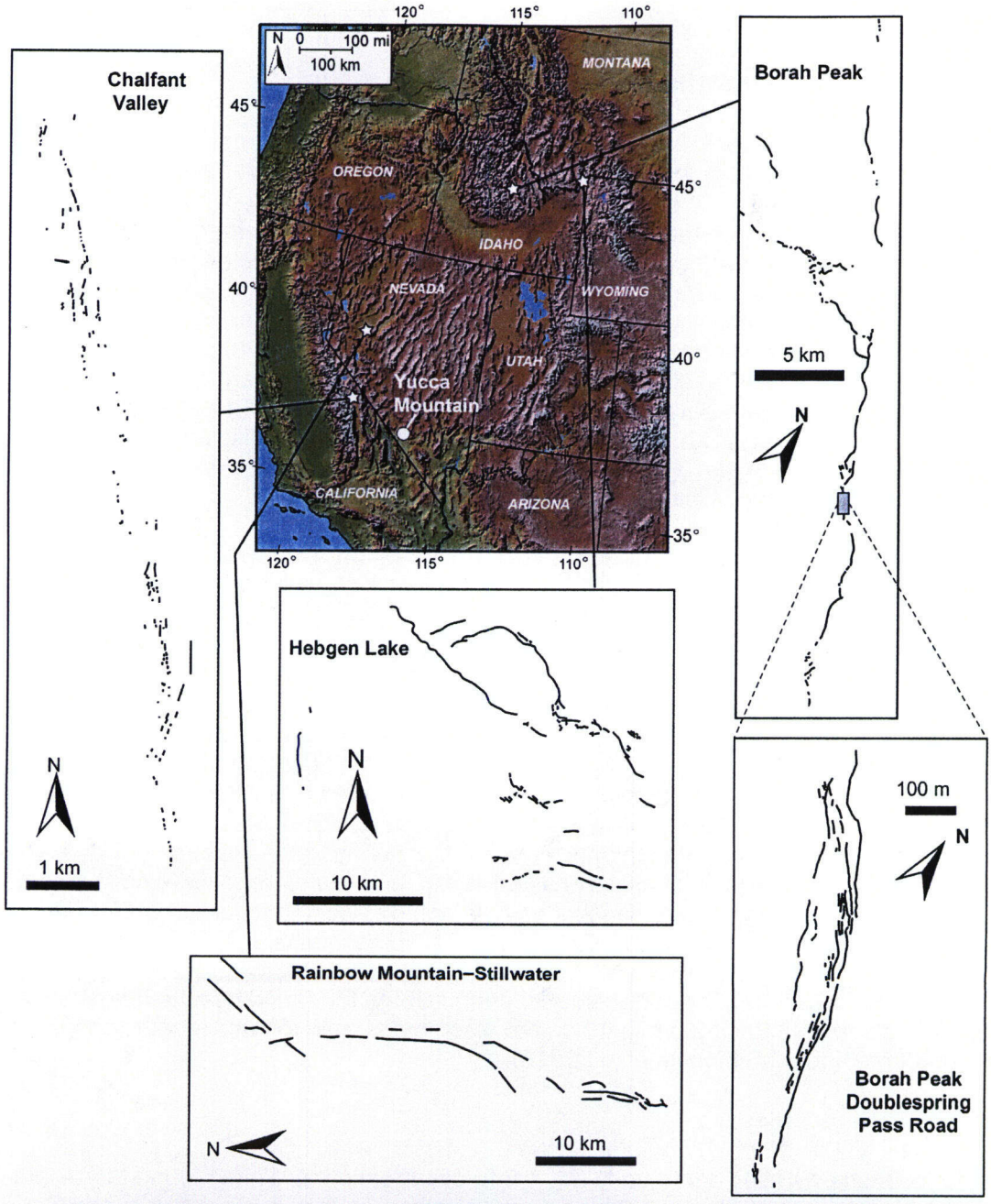

Figure 4-1. Digital Elevation Map Showing the Western United States and Yucca Mountain, Nevada. The Map Also Shows the Location of Four Earthquakes in the Western United States That Produced Ground Rupture. Insets Show Maps of Rupture Traces for Each of the Four Analog Events: Chalfant, Borah Peak, Rainbow Mountain–Stillwater, and Hebgen Lake. Also Shown Is an Inset That Shows a Detailed Portion of the Borah Peak Fault Ruptures near Doublespring Pass Road, Adapted from Crone, et al. (1987).

Individual fracture surface traces trend from 340 to 347°, with a dominant trend of 355°. Associated fault ruptures appeared as narrow 0.05-m- [0.16-ft]-wide fissures or cracks, 0.01–0.02 m [0.03–0.06 ft] wide in fine-grained alluvium or soil. Owing to collapse of surface ruptures, determination of vertical offset was generally not determined, with one fissure showing 0.03 m [0.1 ft] vertical offset. Lienkaemper, et al. (1987) did not report the map scale. Minimum reported displacement trace lengths, however, were tens of meters.

4.1.1.2 Borah Peak

The 1983 Borah Peak earthquake ($\mathbf{M_S}$ = 7.3) occurred along the southwestern boundary of the Lost River Range (Figure 4-1), between Challis and McKay in east-central Idaho (Crone, et al., 1987). The main rupture, with a focal depth of 16 km [9.9 mi], occurred in three sections making a "Y" pattern with a total trace length of 36.4 km [22.6 mi]. The main portion of the surface rupture strikes north-northwest, with southwestward dip of 49 ° (Barrientos, et al., 1987). The southern section, with a trace length of 20.8 km [12.9 mi], is interpreted as the main fault zone. Maximum vertical offset determined from scarp height was 2.7 m [8.9 ft], with a left lateral displacement of 0.7 m [2.3 ft]. Most surface faults displaced unconsolidated alluvium or colluvium and occurred near alluvium-bedrock contact. The mapping scale for surface displacements is not explicitly reported. For the approximately 0.9-km- [0.6-mi]-long segment of the Borah Peak main rupture near Doublespring Pass Road, however, displacement maps are published at scales as detailed as approximately 1:6,500, with a smallest reported trace length of 10–15 m [32.8–49.2 ft] (Crone, et al., 1987).

4.1.1.3 Rainbow Mountain–Stillwater

The 1954 Rainbow Mountain ($\mathbf{M_S}$ = 6.3)–Stillwater ($\mathbf{M_S}$ = 7.0) earthquakes occurred along the eastern base of Rainbow Mountain and the western front of the Stillwater Range, in west-central Nevada (Figure 4-1) (dePolo, et al., 1991). The Rainbow Mountain earthquake preceded the Stillwater earthquake by 48 days. Surface ruptures from the 18 km [11.2 mi] Rainbow Mountain and 45 km [27.9 mi] Stillwater overlapped to form a total surface trace length of 52 km [32.3 mi]. Trends of the surface fault trace were predominantly north-northeast, with some segments trending nearly north. Maximum scarp height was 0.76 m [2.5 ft], and displacement was normal dip slip. Most surface ruptures were in 12,000-year-old Lake Lahonton sediments. The mapping scale for surface ruptures is not known. Displacement traces for this study were taken from dePolo, et al. (1991) at a scale of approximately 1:55,555.

4.1.1.4 Hebgen Lake

The 1959 Hebgen Lake earthquake ($\mathbf{M_S}$ = 7.5) occurred along the Red Canyon and Hebgen faults in southwestern Montana (Figure 4-1) (dePolo, et al., 1991; Hill and Bartholomew, 1999). Total surface rupture trace length on the *en echelon* arranged Red Canyon and Hebgen fault system was 28 km [17.4 mi]. Focal depth is estimated at between 15 and 25 km [9.3 and 15.5 mi]. Trend of the surface rupture system was predominantly north-northwest. Barrientos, et al. (1987) report a main rupture plane strike of 126° with a southwest dip of 50°. Maximum vertical offset (i.e., throw) across the surface rupture system was 4.6 m [15.1 ft], and displacement was normal dip slip. Associated ruptures with maximum vertical offset of 1 m [3.3 ft] occurred as distant as 11 km [6.8 mi] from the main displacement system. The mapping scale for surface displacements is not known. Fault traces for this study were taken from dePolo, et al. (1991) at a scale of approximately 1:35,700.

4.1.2 Fault Trace-Length Density from Historical Faulting in the Western United States

To use the historic displacement maps in this analysis, the map traces of the fault displacements of each analog were used to estimate the spatial density of fault trace-lengths, expressed as a fault trace-length per unit area. This estimation was accomplished using a 100 × 100 m or 10,000 m^2 [328 × 328 ft or 107,639 ft^2] moving window over an orthogonal grid. Fault trace-length densities measured in this way vary between 0 and 45 km/km^2 [0 and 72.4 mi/mi^2] for the four fault displacement patterns analyzed in Figure 4-1. Results of the analysis are shown in Figure 4-2. Mean values for the four maps range between 0.1 and 7.9 km/km^2 [0.2 and 12.7 mi/mi^2].

This type of analysis is sensitive to the scale of observation. The Borah Peak earthquake map at Doublespring Pass Road was mapped at a much finer scale than the other three analogs used in this analysis (Figure 4-1). Thus, the Borah Peak map provides greater detail of surface faulting than the other maps and includes many small secondary faults. As a result, the Borah Peak analog yields the largest fault trace-length densities (Figure 4-2). Similar small faults probably developed as a result of the earthquakes in the other analogs, but these small faults were not mapped because of the coarser map scales. For example, the entire detailed map of the Doublespring Pass Road exposure would be hardly more than a single point on the Rainbow Mountain–Stillwater or Hebgen Lake maps.

The underlying question is whether the analyses under- or over-sampled fault trace-length densities from these fault maps. The critical constraint to this scale-of-observation question is the threshold for fault displacement (i.e., the amount of displacement that could lead to waste package failure within the drifts). As discussed in Section 3.1.4, threshold fault displacements were estimated at 20 cm [0.64 ft] for backfilled drifts and 1.0 m [3.2 ft] for open drifts. Thus, a sufficient sample would include only those faults with displacements greater than 20 cm [0.64 ft] from fault maps drawn at a fine enough scale to ensure that all such faults are adequately represented. The choice of a 100 × 100 m [328 × 328 ft] sample window yields results that should be meaningful at the scale of the proposed drift spacing {approximately 80 m [262.5 ft]} larger sample windows decrease the values of fault density whereas smaller sample windows create bimodal distributions of very low and very high fault densities.

Unfortunately, fault displacements for each fault trace in the four analog maps shown in Figure 4-1 were not provided by the authors, nor were fault displacement criteria used as a basis to include or exclude fault traces from these maps. Thus, it is not known how many of the fault traces in these maps have displacements that exceed the 0.20-m- [0.67-ft]- and 1.0-m- [3.2-ft]-threshold fault displacement. Photographs of faulting at Doublespring Pass Road in the Borah Peak example in Crone, et al. (1997) indicate that some faults with displacement less than 20 cm [0.62 ft] were included in this detailed map. It seems less likely that fault traces with less than 20 cm [0.64 ft] of displacement were included in the Hebgen Lake, Rainbow Mountain–Stillwater, or Chalfant Valley maps given their coarse scale. What is unknown is whether a significant number of secondary faults are missing from these coarser-scale maps.

To constrain the analog earthquake data, fault traces mapped at Yucca Mountain in the vicinity of the proposed repository (Figure 4-3) by Day, et al. (1998a,b) were analyzed. These faults exhibit fault trace-length densities between 0 and 86 km/km^2 [0 and 135.8 mi/mi^2]. The overall fault trace-length density for this analysis at Yucca Mountain is 4.7 km/km^2 [7.6 mi/mi^2]. According to Day, et al. (1998a,b), the criterion for including faults was a minimum threshold

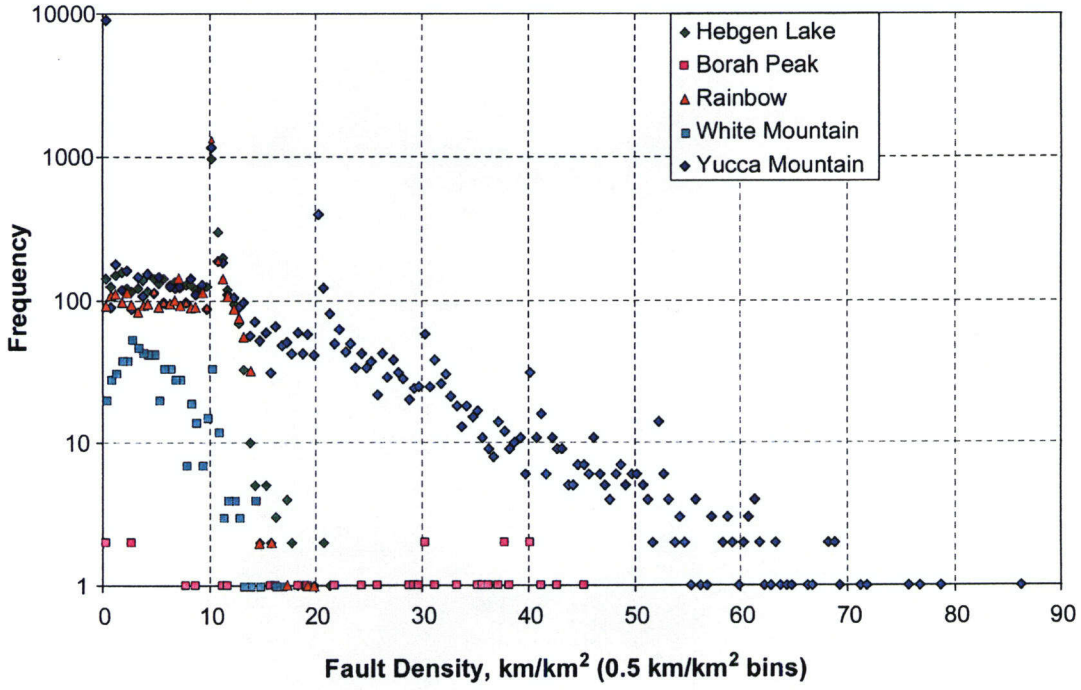

Figure 4-2. Frequency Plot Showing Fault Trace-Length Densities for Distributed Faulting from Recent Earthquakes in the Western United States Compared to the Fault Trace-Length Densities for Yucca Mountain. The Yucca Mountain Analysis Is Based on the Bedrock Geologic Maps of Day, et al. (1998a,b). To Convert to English Units, Multiply Fault Densities by 1.61.

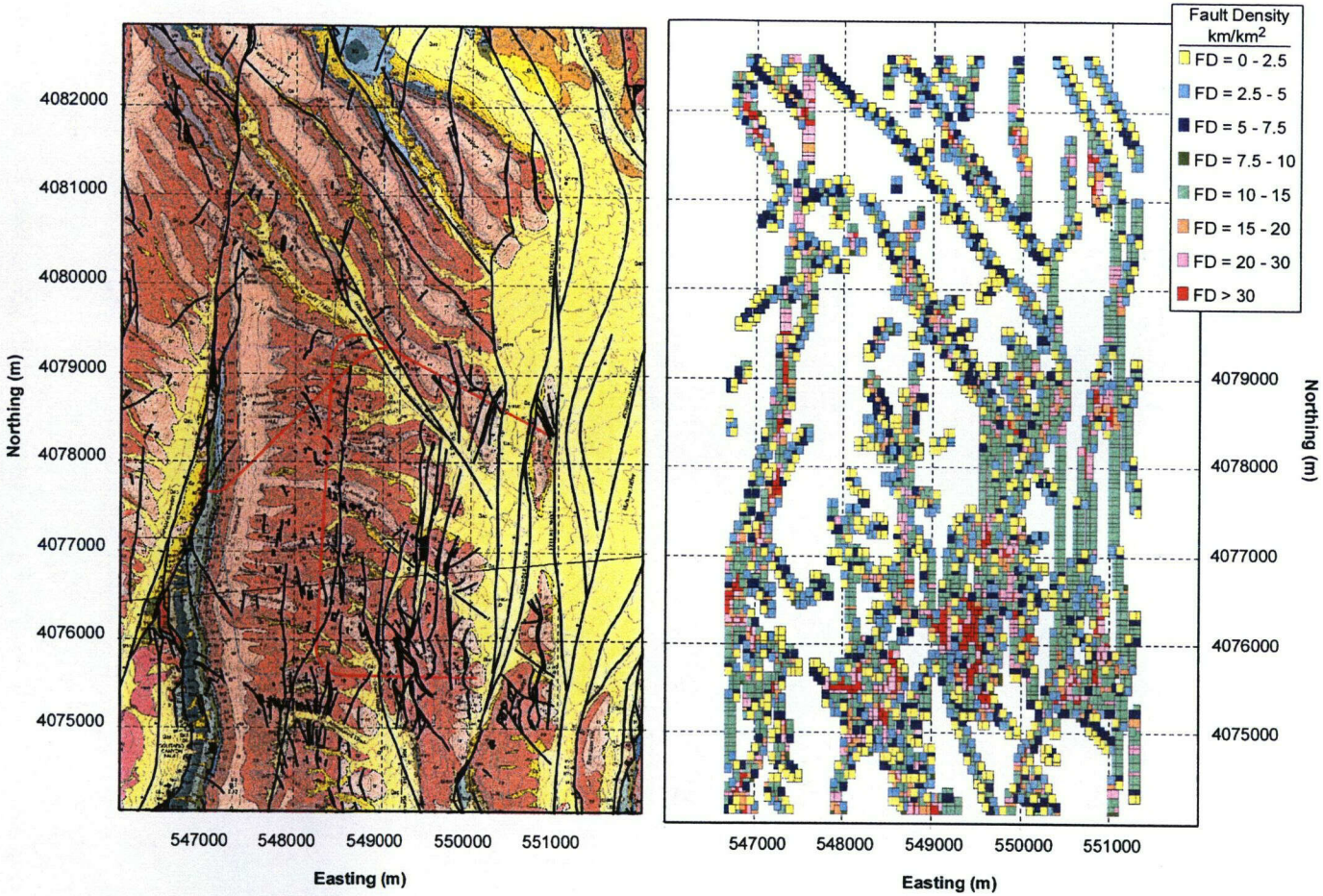

Figure 4-3. Fault Trace-Length Densities at Yucca Mountain Calculated from Mapped Faults. The Left Panel Shows the Geology of the Yucca Mountain Area, from Day, et al. (1998a,b). The Red Lines Shown the Location of the Exploratory Studies Facility and the Cross Drift. Black Lines Are the Mapped Fault Traces. The Right Panel Is a Map of Fault Densities at Yucca Mountain, Based on the Day, et al. (1998a,b) Maps. Grid Spacing is 100 × 100 m^2 [328 × 328 ft^2]. Both Maps are Drawn at the Same Scale.

vertical displacement of approximately 3 m [10 ft] on faults outside the central block and approximately 1.5 m [5.0 ft] for areas inside the central block. Unlike the historic earthquakes, however, the Yucca Mountain faults represent the aggregation of fault slip since the inception of faulting more than 10 million years ago, and, thus, many of these faults incorporate the accumulated deformation of many earthquake cycles.

Although it is unlikely all mapped faults at Yucca Mountain would be activated during a single event, analysis of these faults provides a reasonable if not conservative estimate of the spatial density of distributed faulting—an estimate based directly on the geology and history of faulting at Yucca Mountain. This estimate is consistent with the range of values determined for the analog earthquakes (Figure 4-2). Therefore, a value of 5 km/km^2 [8 mi/mi^2], the average for faults at Yucca Mountain, was used in the following consequence modeling.

4.1.3 Drift Intersection Analysis

The number of drifts possibly intersected by faulting depends on several geometric characteristics of the faults and engineered drifts. The number of potential fault-drift intersections depends on the spatial density of faults, spacing of the drifts, and azimuth of the drifts relative to the fault traces. To quantify the number of drift intersections for a given faulting event, a geometric model was constructed (Figure 4-4). The fault population is modeled as straight, parallel, equally spaced lines inscribed within a circle so that one line represents a diameter (population A, Figure 4-4a). Engineered drifts are modeled as a second population of straight, parallel, equally spaced lines drawn within the circle so that no line passed through the center of the circle (population B, Figure 4-4a). The number of intersections between the two populations of lines within the circle depends on the spacing of the two populations and the angle between them and can be approximated by the relationship:

$$Ni \approx \left[\frac{\sin(\alpha)}{d_B}\right] \times \sum L_A \qquad (4\text{-}1)$$

Where Ni is the number of intersections within the circle, α is the angle between two line populations, $\sum L_A$ is the total line length of fault traces within the circle (population A), and d_B is the spacing of drifts within the circle (population B). Because Ni represents the number of fault-drift intersections, it is an integer value.

Equation 4-1 is written as the line length of one population within the sampled area and the spacing of the other population. This formulation is convenient because the spatial density of distributed fault arrays, which are anastomosing and irregular, is best characterized by the trace length per unit area (as described in the preceding section); whereas, the regular pattern of the drifts is easily represented by drift spacing. Ni can be expressed as the number of drift-fault trace intersections per unit area (divided by the area of the circle). This number can then be used to estimate the total number of intersections for any given area.

The geometric model for evaluating fault-drift intersections is versatile and robust. Shifting the line populations so they are not symmetrically disposed within the circle has little effect on the resulting number of intersections (±1) except in the limiting cases where one or more of the lines in one population is coincident with a line or lines in the other population. In addition, maintaining the total length of population A, but permitting it inconsistent spacing and

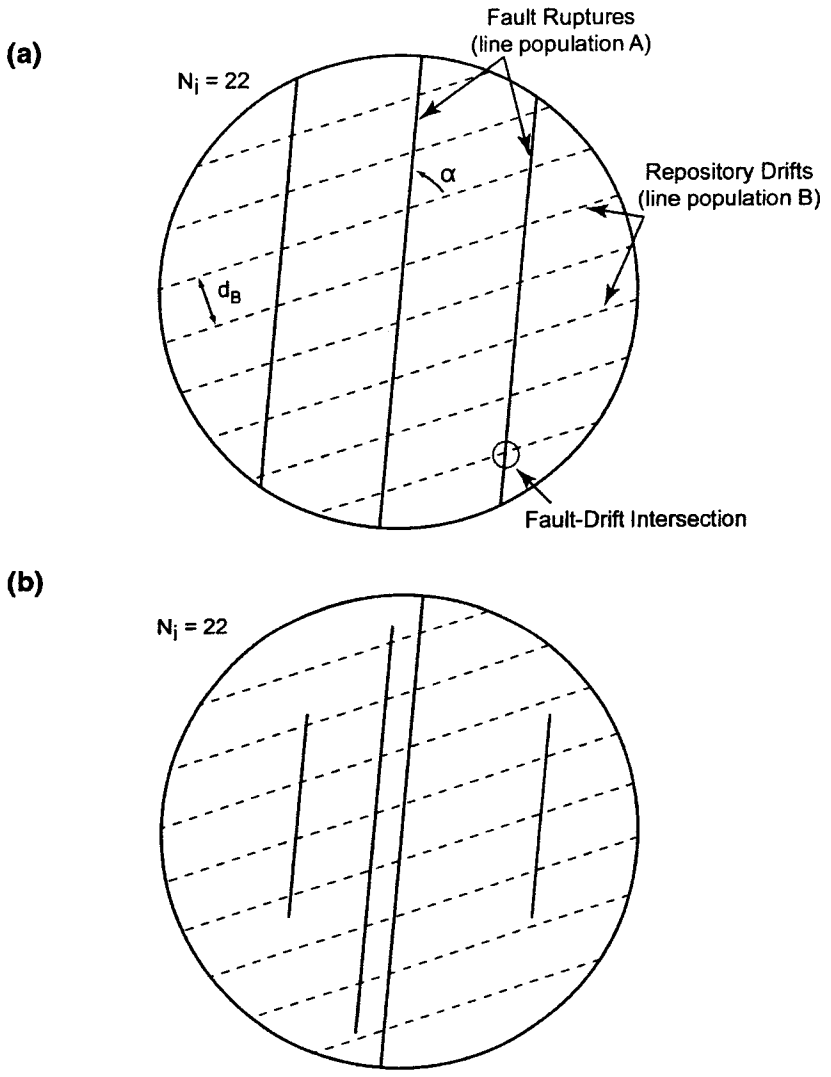

Figure 4-4. Diagram Illustrating the Parameters Used in Eq. 4-1, in Which the Number of Drift-Fault Intersections Is Estimated Based on the Number and Orientation of Faults and the Orientation and Spacing of Repository Drifts. In Both Examples Shown in (a) and (b), the Number of Fault-Drift Intersections (Ni) Is Equal to 22.

distribution (i.e., lines terminating within the circle and not at the perimeter), has little effect on the number of drift-fault intersections (±1) (Figure 4-4b).

4.1.4 Estimates of the Number of Fault-Drift Intersections

The most recent repository design (Figure 2-1a) has a drift azimuth of 072° and a drift spacing of 81 m [265.7 ft] (CRWMS M&O, 2002). Given this design and a 005° mean azimuth of faults at Yucca Mountain (Figure 1-3b), the angle α between dominant fault trace and the drift orientation is equal to 67°. From these values, the estimated number of fault-drift intersections likely to result from an earthquake event at Yucca Mountain as a function of fault density and repository area was calculated (Figure 4-5). Total repository area for this recent design depends on the number of panels ultimately used. Current DOE plans indicate that not all the panels shown in this design will be used, and, thus, the repository will encompass an area between 5 km^2 and 7 km^2 [1.9 mi^2 and 2.7 mi^2].

Assuming a distributed fault density of 5 km/km^2 [8 mi/mi^2] that was estimated from the fault density data described in the proceeding section, the graph in Figure 4-5 indicates 143 and 200 fault-drift intersections. If it is assumed that all fault-drift intersections lead to waste package failures, this analysis estimates 143–200 conditional waste package failures could occur from a large faulting event. This value is conditional in that the probability of this faulting event has not yet been taken into account in the calculation. Similar to Methodology I, probability-weighted doses are calculated from the conditional doses and then used to compute the risk.

4.2 Conditional Dose

To determine the conditional dose consequences using Methodology II, the number of potential waste package failures is input to the TPA Version 4.1j code as juvenile failures. For this analysis, the conservative number of 200 waste package failures was used. These failures were forced to occur in all TPA Version 4.1j code realizations at postclosure year 100.

Except for the use of the juvenile failure parameter, other conditions of the TPA Version 4.1j code were the same as those used in the FAULTO module methodology discussed in Chapter 3. The TPA Version 4.1j code run consisted of 500 realizations of the code to ensure statistically reliable results. The beneficial effects of the drip shield were removed as before. The full range of parameters in the standard base case input file was sampled in each realization.

Results of conditional dose versus time for faulting events are shown in Figure 4-6. Similar to those curves shown in Figure 3-2, the dose versus time curves show an initial peak within approximately 2,000 years of the faulting event, indicating an influence of the thermal pulse on initial solubility rates of radionuclides. The curves also show a steady increase in dose, reaching a second maximum at year 10,000. The maximum mean peak conditional dose in this example calculation is 2.9×10^{-5} rem, which occurs at approximately year 3,000.

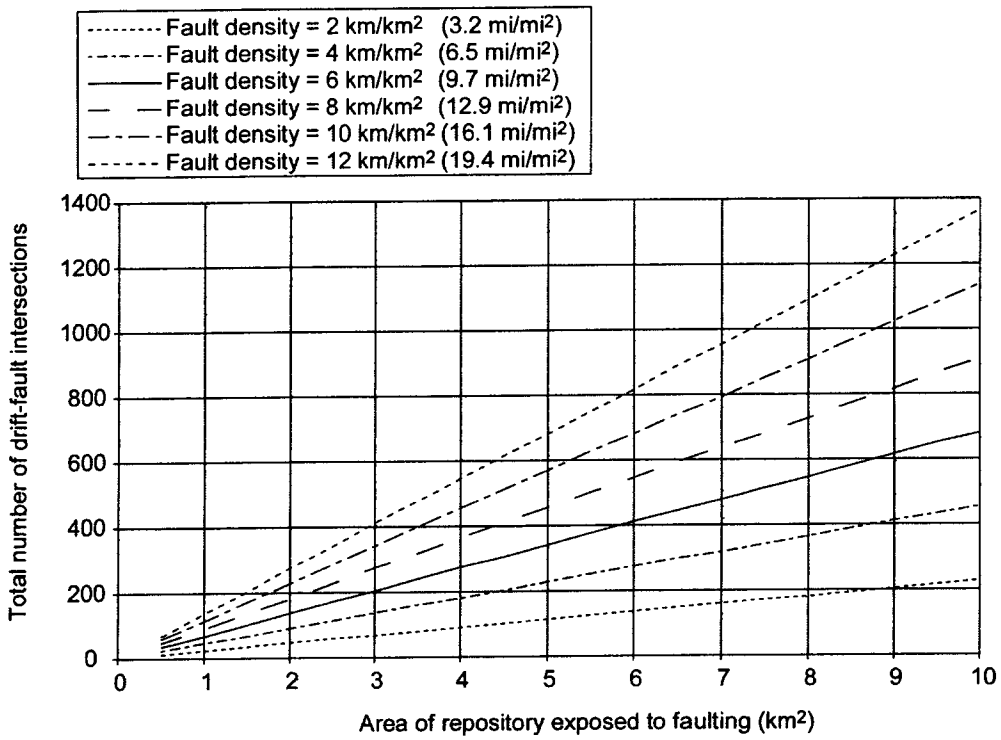

Figure 4-5. Graph of the Total Number of Drift-Fault Intersections for a Series of Fault Density Values As a Function of Repository Area

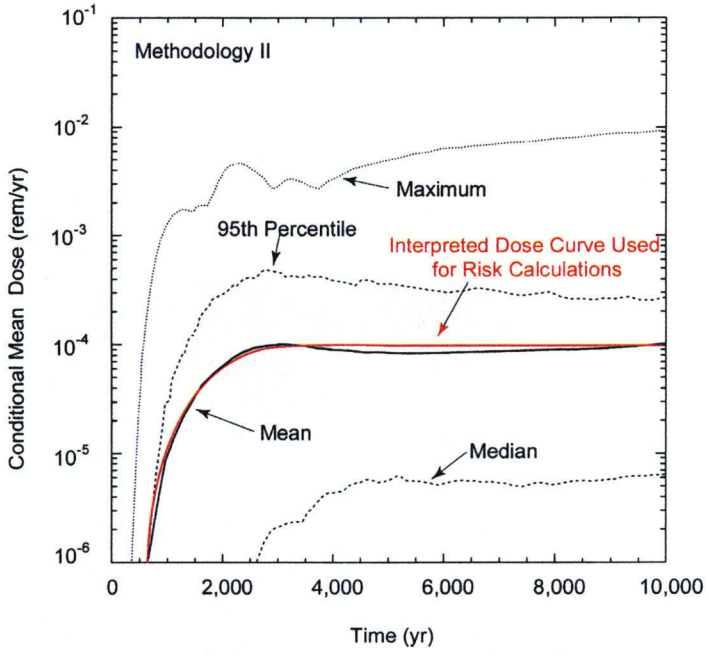

Figure 4-6. Graphical Plots of the Conditional Doses Through Time for Methodology II. Faulting Is Abstracted As Juvenile Failures, Forced to Occur at Year 100. Results Are Presented for the Mean, Median, 95th Percentile, and Maximum Values of 500 Realizations. The Red Curve Is the Interpreted Dose Versus Time Curve Used in the Risk Calculations.

4.3 Risk

4.3.1 Risk Calculation Procedure

The procedures to estimate risk are quite similar to those described in Section 3.3.1. First, the dose versus time curve was enveloped by an interpolated curve that could be used to extrapolate doses for each year between years 100 and 10,000. This best-fit curve consisted of a third order polynomial (Table 4-1) for the first 3,100 years, wherein the doses increase to a maximum value at year 3,000. Dose is then a constant dose value for all years beyond year 3,100 to year 10,000 (Figure 4-6).

Table 4-1. Best-Fit Dose Versus Time Coefficients

Year of Maximum Conditional Mean Peak Dose	Maximum Conditional Mean Peak Dose (rem)	Best-Fit Polynomial Coefficients
3,163	2.9×10^{-5}	$A_0 = 1.58 \times 10^{-6}$ $A_1 = -1.96 \times 10^{-8}$ $A_2 = 2.75 \times 10^{-11}$ $A_3 = 1.37 \times 10^{-14}$

4.3.2 Estimate of Risk

Based on this best-fit curve, conditional doses were derived for each year between years 100 and 10,000, and the probability-weighted doses for each year between years 100 and 10,000 were calculated. The conditional doses were weighed by the probabilities that a faulting event similar to the faulting analogs could occur in the repository at Yucca Mountain. Similar to Methodology I, these probabilities were derived from the DOE probabilistic fault displacement hazard results (CRWMS M&O, 1998a). Risk in year 10,000 was then computed by summing the risks of that year with the risks for all prior years.

For example, maximum fault displacement for the Borah Peak earthquake, as measured by Crone, et al. (1987), was 2.7 m [8.9 ft], with an average displacement of approximately 1 m [3.2 ft]. The mean annual exceedence probabilities for 1 m [2.6 ft] of displacement for faults at Yucca Mountain (CRWMS M&O, 1998) range between 5×10^{-6}/yr for the Solitario Canyon fault to 3×10^{-8}/yr for the Ghost Dance fault. Risk estimates, based on these probabilities, range between 4.0×10^{-6} and 2.4×10^{-8} rem/yr.

4.3.3 Risk Insights

Similar to Methodology I, the risk estimates from Methodology II are based on numerous conservative or pessimistic assumptions about the mechanical behavior of waste packages and the characteristics of faulting at Yucca Mountain. For example

- No credit was taken for the benefits of drip shields. Limitations in the TPA Version 4.1j code do not allow for a direct link between faulted waste package and over-capping drip shields. In the analyses in this report, the drip shields were removed from the engineered system.

- A flow-through model was used to simulate water entering and exiting from damaged waste packages. This model implies that all waste packages are breached in such a way that water can enter and exit immediately after fault slip.

- Failure of the waste packages was assumed for each fault-drift intersection. No credit was taken for the material strength or ductility of the waste package material.

- The amount of fault slip on the analog secondary faults was not a factor in developing the fault trace-length densities used. All mapped fault trace-lengths were counted in the analogs as part of the fault trace-length density estimates. More realistic and detailed mapping, where the smallest secondary faults are screened from the analysis, could yield fewer fault-drift intersections.

- To simplify the risk calculation, risk caused faulting in any year was based on an extrapolation of the mean condition dose versus time curve for the faulting event that occurred at year 100. This extrapolated curve yields larger conditional doses than would occur if actual dose calculations were performed to appropriate postclosure years.

Despite these conservative and pessimistic assumptions, a reasonable upper estimate of the risk imposed by faulting on postclosure repository performance by Methodology II is also small. Similar to Methodology I, risk estimates are on the order of pico-rems to tens of micro-rems per year. As before, the main factor for these low-risk values is the relatively small annual exceedence probabilities for consequential fault displacements at Yucca Mountain (Table 3-2). Similar to Methodology I, the relatively small risks of faulting estimated by this analysis supports the DOE conclusion that direct faulting of the drifts and waste packages is a disruptive event process that can be screened from a total system performance assessment based on low risk significance.

4.4 Limitations to Analog Faulting Methodology

Introduction of the analog faulting models adds geologic realism to the consequence analysis. Nevertheless, as described in the proceeding section, Methodology II necessarily incorporates a variety of simplifying and pessimistic assumptions about the characteristics of faulting at Yucca Mountain and the mechanical behavior of waste packages under anticipated faulting loads. For example, additional detailed analyses of historic faulting data may yield a better understanding of distributed faulting that could affect drifts and waste packages and thereby reduce uncertainty in the models. In addition, a more complete abstraction of the mechanical failure of the waste packages would make faulting consequence modeling more realistic. Additional realism also could be gained by incorporating the drip shields into the faulting and mechanical response analysis. Because this demonstrably conservative risk assessment indicates only minor risk significance associated with postclosure faulting, however, additional sophistication in the modeling does not appear warranted.

5 CONCLUSIONS

Staff evaluated the current DOE analyses of direct fault displacement of waste packages as a disruptive event within the overall assessment of postclosure performance for the proposed Yucca Mountain repository. This evaluation includes a review of the DOE probabilistic fault displacement results and associated DOE analyses of the potential consequences of faulting. Based on this review of the DOE analyses, coupled with risk insights gained from an independent consequence analysis of fault displacement of waste packages, staff conclude DOE has assembled sufficient information in the prelicensing period on the issue of direct faulting for the NRC staff to conduct a review of a potential License Application. Therefore, staff consider the faulting subissue, as defined within the Structural Deformation and Seismicity Key Technical Issue, to be closed. The narrow definition of faulting (i.e., direct fault displacement of waste packages) excludes other possible coupled effects of faulting such as fault-induced modifications to groundwater flow, rockfall, or enhanced corrosion of the engineered barrier system due to rock–waste package interactions. These other fault-related scenarios will be considered and addressed separately in other disruptive events analyses and evaluations.

As part of the staff review of the DOE approach and results, staff developed two alternative methodologies that can be used to independently evaluate the potential consequences of fault disruption of the waste packages and drip shields. The first methodology is based on an abstraction of faulting within the TPA Version 4.1j code: faulting parameters derived from geological data. The second method is a more detailed process model based on patterns of primary and secondary faults from historic large-magnitude earthquakes in the Basin and Range.

At present, both alternative methodologies rely on numerous pessimistic or conservative assumptions about the nature of faulting and the mechanical behavior of waste packages under faulting loads. These assumptions include minimum fault displacement thresholds for waste package damage, no credit for the drip shields, and no credit for the mechanical strength of the waste packages once they are impinged within the drifts by faulting. These simplifying assumptions were necessary to develop efficient and understandable abstractions of the complex natural system. Therefore, results from both methodologies are considered to provide reasonably conservative estimates of the number of potential waste package failures in the event of fault displacements and associated dose consequences. If faulting is subsequently shown to make a significant contribution to overall repository risk, the faulting performance assessment methodologies developed in this report should be refined to capture greater realism.

Despite these conservative or pessimistic assumptions, the risks imposed by waste package rupture by fault slip on postclosure repository performance appear to be small, on the order of pico-rem to tens of micro-rems per year. The two principal factors controlling these low-risk values are the relatively small annual exceedence probabilities for consequential fault displacements at Yucca Mountain and the fact that relatively few waste packages are impacted by faulting. Risk insights of faulting, therefore, support the DOE conclusion that direct faulting of the drifts and waste packages is a disruptive event process that can be screened from the TPA Version 4.1j code based on low risk significance. Based on these risk insights, coupled with a detailed review of current DOE information on the probability and consequences of faulting, staff conclude the faulting subissue, as defined within the Structural Deformation and Seismicity Key Technical Issue, is closed.

6 REFERENCES

Barrientos, S.E., R.E. Stein, and S.N. Ward. "Comparison of the 1959 Hebgen Lake, Montana, and the 1983 Borah Peak, Idaho, Earthquakes from Geodetic Observations." *Bulletin of the Seismological Society of America*. Vol. 77, No. 3. pp. 784–808. 1987.

Bell, J.W. "Quaternary Fault Map of the Nevada–Reno Sheet." Nevada Bureau of Mines and Geology. Map 79. Scale 1:250,000. 1984.

Burchfiel, B.C. "Structural Geology of the Specter Range Quadrangle, Nevada, and Its Regional Significance." *Geological Society of America Bulletin*. Vol. 76. pp. 175–192. Scale 1:62,500. 1965.

Cockerham, R.S. and E.J. Corbett. "The 1986 Chalfant Valley, California, Earthquake Sequence." *Bulletin of the Seismological Society of America*. Vol. 77. pp. 280–289. 1987.

Coppersmith, K.J. "Update on Data Related to Fault Displacement and Vibratory Ground Motion Hazard at Yucca Mountain for Use in EPRI Performance Assessment in Yucca Mountain Total System Performance Assessment, Phase 3." J. Kessler and R. McGuire, eds. EPRI TR–107191 3055-02 Final Report. Palo Alto, California: Electric Power and Research Institute. pp. 11-1 to 11-15. 1996.

Crone, A.J., M.N. Machette, M.G. Bonilla, J.J. Lienkaemper, K.L. Pierce, W.E. Scott, and R.C. Bucknam. "Surface Faulting Accompanying the Borah Peak Earthquake and Segmentation of the Lost River Fault, Central Idaho." *Bulletin of the Seismological Society of America*. Vol. 77, No. 3. pp. 739–770. 1987.

CRWMS M&O. "Underground Layout Configuration: Subsurface Tunneling and Emplacement Drift Systems." 800–P0C–MGR0–00100–000–00A. Las Vegas, Nevada: CRWMS M&O. 2002.

———. "Disruptive Events Process Model Report." TDR–NBS–MD–000002. Rev. 00 ICN 01. Las Vegas, Nevada: CRWMS M&O. 2000a.

———. "Yucca Mountain Site Description." TDR–CRW–GS–000001. Rev. 01 ICN 01a. Las Vegas, Nevada: CRWMS M&O. 2000b.

———. "Features, Events, and Processes: Disruptive Events." ANL–WIS–MD–000005. Rev. 00 ICN 01. Las Vegas, Nevada: CRWMS M&O. 2000c.

———. "Characterize Framework for Seismicity and Structural Deformation at Yucca Mountain, Nevada." ANL–CRW–GS–000003. Rev. 00. Las Vegas, Nevada: CRWMS M&O. 2000d.

———. "Effects of Fault Displacement on Emplacement Drifts." ANL–EBS–GE–000004. Rev. 00 ICN 01. Las Vegas, Nevada: CRWMS M&O. 2000e.

———. "Total System Performance Assessment for the Site Recommendation." TDR–WIS–PA–000001. Rev. 00 ICN 01. Las Vegas, Nevada: CRWMS M&O. 2000f.

———. "Probabilistic Seismic Hazard Analyses for Fault Displacement and Vibratory Ground Motion at Yucca Mountain, Nevada." WBS 1.2.3.2.8.3.6. Oakland, California: DOE. 1998a.

———. "Viability Assessment of a Repository at Yucca Mountain. Vol. 3: Total System Performance Assessment." DOE /RW–0508/V3. Las Vegas, Nevada: DOE, Office of Civilian Radioactive Waste Management. 1998b.

Day, W.C., R.P. Dickerson, C.J. Potter, D.S. Sweetkind, C.A. San Juan, R.M. Drake, II, and C.J. Fridrich. "Geologic Map of the Yucca Mountain Area, Nye County, Nevada." U.S. Geological Survey Geologic Investigations Series, Map I–2627. Scale 1:24,000. 1998a.

Day, W.C., C.J. Potter, D.S. Sweetkind, R.P. Dickerson, and C.A. San Juan. "Bedrock Geologic Map of the Central Block Area, Yucca Mountain, Nye County, Nevada." U.S. Geological Survey Miscellaneous Investigations Series, Map I–2601. Scale 1:6,000. 1998b.

dePolo, C.M., D.G. Clark, D.B. Slemmons, and A.R. Ramelli. "Historical Surface Faulting in the Basin and Range Province, Western North America, Implications for Fault Segmentation." *Journal of Structural Geology*. Vol. 13. pp. 123–126. 1991.

Ferrill, D.A., J.A. Stamatakos, and D. Sims. "Normal Fault Corrugation: Implications for Growth and Seismicity of Active Normal Faults." *Journal of Structural Geology*. Vol. 21. pp. 1,027–1,038. 1999.

Ghosh, A., R.D. Manteufel, and G.L. Stirewalt. "Faulting Version 1.0—A Code for Simulation of Direct Fault Disruption: Technical Description and User's Guide." San Antonio, Texas: CNWRA. 1997.

Ghosh, A., J.A. Stamatakos, S. Hsiung, R. Chen, A.H. Chowdhury, and H.L. McKague. "Key Technical Issue Sensitivity Analysis with Seismo and FAULTO Modules within the TPA (Version 3.1.1) Code." San Antonio, Texas: CNWRA. 1998.

Gray, M.B., J.A. Stamatakos, and D.A. Ferrill. "Microstructural and Microtextural Analyses of Faulting at Yucca Mountain, Nevada." *EOS, Transactions of the American Geophysical Union*. Vol. 79, No. 45. pp. F823. 1998.

Hanks, T.C. and D.P Schwartz. "Morphologic Dating of the Pre-1983 Fault Scarp on the Lost River Fault at Doublespring Pass Road, Custer County, Idaho." *Bulletin of the Seismological Society of America*. Vol. 77, No. 3. pp. 837–846. 1987.

Harmsen, S.C. "The Little Skull Mountain, Nevada, Earthquake of 29 June 1992: Aftershock Focal Mechanisms and Tectonic Stress Field Implications." *Bulletin of the Seismological Society of America*. Vol. 84. pp. 1,484–1,505. 1994.

Hill, A.A. and M.J. Bartholomew. "Seismic Hazard Susceptibility in Southwestern Montana: Comparison at Dillon and Bozeman." *Guidebook to the Geology of Eastern Idaho*. S.S. Hughes and G.D. Thackray, eds. Pocatello, Idaho: Museum of Natural History. pp. 131–140. 1999.

Lienkaemper, J.J., S.K. Pezzopane, M.C. Clark, and M.J. Rymer. "Fault Fractures Formed in Association with the 1986 Chalfant Valley, California, Earthquake Sequence: Preliminary Report." *Bulletin of the Seismological Society of America*. Vol. 77, No. 1. pp. 297–305. 1987.

McLaren, M.K. and W.U. Savage. "Seismicity of South-Central Coastal California: October 1987 through January 1997." *Bulletin of the Seismological Society of America*. Vol. 91. pp. 1,629–1,658. 2001.

Mohanty, S., R. Codell, J.M. Menchaca, R.Janetzke, M. Smith, P. LaPlante, M. Rahimi, and A. Lozana. "System-Level Performance Assessment of the Proposed Repository at Yucca Mountain Using the TPA Version 4.1 Code." CNWRA 2002-05. Rev. 1.0. San Antonio, Texas: CNWRA. 2002a.

Mohanty, S., T.J. McCartin, and D.W. Esh. "Total-system Performance Assessment (TPA) Version 4.0 Code: Module Description and User's Guide." San Antonio, Texas: CNWRA. 2002b.

Mongano, G.S., W.L. Singleton, T.C. Moyer, S.C. Beason, G.L.W. Eatman, A.L. Algin, and R.C. Lung. "Geology of the Enhanced Characterization of the Repository Block Cross Drift—Exploratory Studies Facility, Yucca Mountain, Nevada." http://www.ymp.gov/timeline/site/spg42gm3_a/. 1999.

Morris, A.P., D.A. Ferrill, and D.B. Henderson. "Slip-Tendency Analysis and Fault Reactivation." *Geology*. Vol. 24. pp. 275–278. 1996.

NRC. NUREG–1762, "Integrated Issue Resolution Status Report." Washington, DC: NRC. July 2002a.

———. NUREG–1804, "Yucca Mountain Review Plan—Draft Report for Comments." Rev. 2. Washington DC: NRC. March 2002b.

———. "Issue Resolution Status Report, Key Technical Issue: Structural Deformation and Seismicity." Rev. 2. Washington DC: NRC. 1999.

Savage, J.C., M. Lisowski, W.K. Gross, N.E. King, and J.L. Svarc. "Strain Accumulation Near Yucca Mountain, Nevada, 1983–1993." *Journal of Geophysical Research*. Vol. 99. pp. 18,103–18,107. 1994.

Simonds, W.F., J.W. Whitney, K. Fox, A. Ramelli, J.C. Yount, M.D. Carr, C.D. Menges, R. Dickerson, and R.B. Scott. "Map of Fault Activity of the Yucca Mountain Area, Nye County, Nevada." U.S. Geological Survey Miscellaneous Investigations Series, Map I–2520. Scale 1:24,000. 1995.

Sims, D., D.A. Ferrill, and J.A. Stamatakos. "Role of Ductile Décollement in the Development of Pull-Apart Basins: Experimental Results and Natural Examples." *Journal of Structural Geology*. Vol. 21. pp. 533–554. 1999.

Smith, K.D. and K.F. Priestley. "Faulting in the 1986 Chalfant, California, Sequence: Local Tectonics and Earthquake Source Parameters." *Bulletin of the Seismological Society of America*. Vol. 90. pp. 813–831. 2000.

Stepp, J.C. and C.A. Cornell. "Approach to Postclosure Seismic Analyses for a Potential Geological Repository at Yucca Mountain, Nevada." Letter Report. Washington, DC: DOE, Site Characterization Office. 2001.

Stewart, J.H. "Tectonics of the Walker Lane Belt, Western Great Basin—Mesozoic and Cenozoic Deformation in a Zone of Shear." *Metamorphism and Crustal Evolution of the Western United States, Rubey Volume*. W.G. Ernst, ed. Englewood Cliffs, New Jersey: Prentice Hall. pp. 683–713. 1988.

———. "Basin-Range Structure in Western North America: A Review." *Cenozoic Tectonic and Regional Geophysics of the Western Cordillera*. R.B. Smith and G.P. Eaton, eds. *Geological Society of America Memoir 152*. Boulder, Colorado: Geological Society of America. pp. 1–31. 1978.

Tchalenko, J.S. and N.N. Ambraseys. "Structural Analysis of the Dasht-e Bayly (Iran) Earthquake Fractures." *Geological Society of America Bulletin*. Vol. 81. pp. 41–60. 1970.

Tocher, C. "Movement on the Rainbow Mountain Fault." *Bulletin of the Seismology Society of America*. Vol. 46. pp. 10-14. 1956.

U.S. Geological Survey. "Seismotectonic Framework and Characterization of Faulting at Yucca Mountain, Nevada." J.W. Whitney, coord. Denver, Colorado: U.S. Geological Survey. 1996.

———. "The Hebgen Lake, Montana, Earthquake of August 17, 1959." *U.S. Geological Survey Professional Paper 435*. Denver, Colorado: U.S. Geological Survey. 1964.

Wells, D.L. and K.J. Coppersmith. "New Empirical Relationships among Magnitude, Rupture Length, Rupture Width, Rupture Area, and Surface Displacement." *Bulletin of the Seismological Society of America*. Vol. 84. pp. 974–1,002. 1994.

Woodcock, N.J. and M. Fischer. "Strike-Slip Duplexes." *Journal of Structural Geology*. Vol. 8. pp. 725–735. 1986.

Youngs, R.R. and K.J. Coppersmith. "Implications of Fault Slip Rates and Earthquake Recurrence Models to Probabilistic Seismic Hazard Estimates." *Bulletin of the Seismological Society of America*. Vol. 75. pp. 939–964. 1985.

Youngs, R.R., W.J. Arabasz, R.E. Anderson, A.R. Ramelli, J.P. Ake, D.B. Slemmons, J.P McCalpin, D.I. Doser, C.J. Fridrich, F.H. Swan, III, A.M. Rogers, J.C. Yount, L.W. Anderson, K.D. Smith, R.L. Bruhn, P.L Knuepfer, R.B. Smith, C.M. dePolo, D.W. O'Leary, K.J. Coppersmith, S.K. Pezzopane, D.P. Schwartz, J.W. Whitney, S.S. Olig, and G.R. Toro. "A Methodology for Probabilistic Fault Displacement Hazard Analyses (PFDHA)." *Earthquake Spectra*. Vol. 19, No. 1. pp. 191–219. 2003.